

Draft Manuscript for Review

Geochemical evolution of arc and slab following subduction initiation: a record from the Bonin Islands, Japan

Journal:	<i>Journal of Petrology</i>
Manuscript ID	JPET-Feb-20-0021.R2
Manuscript Type:	Original Manuscript
Date Submitted by the Author:	27-Apr-2020
Complete List of Authors:	Ishizuka, Osamu; National Institute of Advanced Industrial Science and Technology Geological Survey of Japan, Taylor, Rex; University of Southampton Faculty of Natural and Environmental Sciences Umino, Susumu; Kanazawa University Graduate School of Natural Science and Technology Kanayama, Kyoko; Tottori Prefecture
Keyword:	subduction initiation, boninite, geochemistry, Bonin Islands, Izu-Bonin-Mariana arc

SCHOLARONE™
Manuscripts

1
2
3
4
5
6 **1 Geochemical evolution of arc and slab following subduction initiation: a record from the**
7 **2 Bonin Islands, Japan**
8

9
10
11 4 Osamu Ishizuka*

12 5 Institute of Earthquake and Volcano Geology, Geological Survey of Japan, AIST, Central 7, 1-1-1, Higashi,
13 6 Tsukuba, Ibaraki, 305-8567, Japan. e-mail address: o-ishizuka@aist.go.jp Phone: +81-29-861-3828, Fax: +81-
14 7 29-856-8725

15
16
17 8 Also at: Japan Agency for Marine-Earth Science and Technology, 2-15 Natsushima, Yokosuka, Kanagawa, 237-
18 9 0061, Japan

19
20
21 10 Rex N. Taylor

22 11 School of Ocean and Earth Sciences, University of Southampton, Waterfront Campus, Southampton, SO14 3ZH,
23 12 UK. E-mail: rex@soton.ac.uk

24
25
26 13 Susumu Umino

27 14 Division of Natural System, Kanazawa University, Kanazawa, Ishikawa 920-1192, Japan. E-mail:
28 15 sesumin@staff.kanazawa-u.ac.jp

29
30
31 16 Kyoko Kanayama

32 17 Tottori Prefecture, Iwami, Tottori, 681-0001, Japan E-mail: kanayamak@pref.tottori.lg.jp
33
34
35
36
37
38
39
40
41
42
43
44
45
46
47
48
49
50
51
52
53
54
55

56 31 Running title: Arc magma evolution after subduction initiation
57 32
58
59 33 *corresponding author
60

1
2
3
4
5
6 34 **ABSTRACT**

7 35 Volcanism following the initiation of subduction is vital to our understanding of this specific
8 36 magma-generation environment. This setting is represented by the first development of the Izu-
9 37 Bonin-Mariana arc system as subduction commenced along the Western Pacific margin in the
10 38 Eocene. A new collection of volcanics recovered from the islands and exposed crustal sections
11 39 of the Bonin Ridge span the first 10 Myr of arc evolution. An elemental and radiogenic isotope
12 40 dataset from this material is presented in conjunction with new $^{40}\text{Ar}/^{39}\text{Ar}$ ages and a stratigraphic
13 41 framework developed by a detailed mapping campaign through the volcanic sections of the
14 42 Bonin Islands.

15 43 The dating results reveal that both the locus and type of magmatism systematically changed
16 44 with time in response to the progressive sinking of the slab until the establishment of steady-
17 45 state subduction at around 7-8 Myr. Following initial MORB-like spreading-related basalt
18 46 magmatism, volcanic centres migrated away from the trench and changed from high-Si boninite
19 47 to low-Si boninite/high-Mg andesite, then finally tholeiitic/calcalkaline arc magma.

20 48 Subducting pelagic sediment combined with Pacific-type igneous ocean crust dominate the
21 49 slab input to the shallow source of high-Si boninites at 49 Ma, but high-precision Pb isotope
22 50 data show that this sediment varies in composition along the subducting plate. At around 45
23 51 Ma, volcanism switched to low-Si boninite and the pelagic sediment signature was almost
24 52 entirely replaced by volcanic or volcanoclastic material originating from a HIMU ocean island
25 53 source. These low-Si boninites are isotopically consistent with a slab component comprising
26 54 variable proportions of HIMU volcanoclastics and Pacific MORB. In turn, this signature was
27 55 replaced by a Pacific MORB-dominated flux in the post 45 Ma tholeiite and calcalkaline
28 56 volcanics. Notably, each change in slab-derived flux coincided with a change in the magma
29 57 type.

30 58 Fluctuations in the slab-derived geochemical signature were superimposed on a change in
31 59 the mantle wedge source from highly-depleted harzburgite to a depleted MORB-type mantle-
32 60 type source. In turn, this may correspond to the increasing depth of the leading edge of the slab
33 61 through this 5 Myr period.

34 62

35 63

36 64

37 65

38 66 Key words: subduction initiation; boninite; geochemistry; Bonin Islands; Izu-Bonin-Mariana
39 67 arc

40 68

41 69

42 70

68 INTRODUCTION

69
70 Subduction initiation and the subsequent development of oceanic island arcs are poorly
71 understood and remain an important unresolved problem in plate tectonics (e.g., Stern, 2004).
72 Stern *et al.* (2012) emphasized the importance of studying forearc sections, which are not
73 masked by younger sediment or accreted material from the subducting plate, to elucidate
74 processes at subduction initiation. Recent geological and geophysical surveys of the trenchward
75 Izu-Bonin-Mariana forearc, in sections such as the Bonin Ridge and SE of Guam, have revealed
76 that their crustal stratigraphy was generated during the initial stages of arc formation (e.g.,
77 Ishizuka *et al.*, 2006a, 2011a, 2014a; Reagan *et al.*, 2010, 2017). These forearc crustal sections
78 span ~1200 km along the arc, yet have quite consistent stratigraphic sequences, which from
79 bottom to top are: 1) gabbroic rocks, 2) a sheeted dyke complex, 3) basaltic lava flows, 4) lava
80 flows, dykes and volcanoclastics of boninite and tholeiitic andesite, and 5) tholeiitic and
81 calcalkaline basalt to andesite. In addition to the crustal section, dredge sampling and ROV
82 dives recovered mantle peridotite beneath the gabbro. These observations indicate that almost
83 all of the forearc crust down to Moho has been preserved in this forearc area.

84 Based on these subaerial and submarine studies of the trenchward forearc, processes at
85 subduction initiation have to some extent become clearer. Subduction along the Izu-Bonin-
86 Mariana arc is estimated to have initiated at c. 52 Ma. The onset of slab sinking and the
87 associated counterflow of asthenospheric mantle resulted in seafloor spreading on the
88 overriding plate, which generated the first volcanism in the form of forearc basalts (FAB:
89 Reagan *et al.*, 2010). These eruptions are followed at ~46-50 Ma by boninitic magmatism, and
90 then tholeiitic and calcalkaline magmatism at ~44-45 Ma. A comprehensive record of the
91 boninitic and subsequent early arc tholeiitic to calcalkaline arc magmatism is preserved and
92 exposed on the Bonin Islands (Umino, 1985; Umino & Nakano, 2007; Umino *et al.*, 2009,
93 2016; Kanayama *et al.*, 2012, 2014).

94 This outline model for subduction initiation described above needs to be tested by
95 determining the nature and composition of the subduction-derived material and the local sub-
96 crustal mantle during the magmatic development. Taylor *et al.* (1994) showed that boninites
97 from the Chichijima Island have uniquely low Sm/Zr and Ti/Zr, and along with other
98 geochemical characteristics of boninites, they implied that slab melts with residual amphibole
99 might contribute to boninite magma as well as a variably depleted mantle source. Kanayama *et al.*
100 (2012) also found that the same processes generated the boninites from the Mukojima
101 Islands. Umino *et al.* (2015, 2018) analysed primitive melt inclusions in chrome spinel and
102 recognised two types of boninite magma. Temperature-pressure conditions for primary
103 boninites, which range from 1345°C at 0.56 GPa to 1421°C at 0.85 GPa for the 46–48 Ma low-

1
2
3
4
5
6 104 Si and high-Si boninites, and 1381°C at 0.85 GPa for the 45 Ma low-Si boninite. They suggested
7 105 that at 46–48 Ma, introduction of slab fluids induced melting of the residue of preceding basaltic
8 106 magmatism (FAB) and high-temperature harzburgite, resulting in the low-Si and high-Si
9 107 boninites, respectively. By 45 Ma, convection within the mantle wedge brought the less-
10 108 depleted residue of FAB and depleted MORB-type mantle (DMM) into the region fluxed by
11 109 slab fluids, which melted to yield the less-depleted low-Si boninite, and more fertile arc basalts,
12 110 respectively.

13 111 The composition of early arc magmatism is also a function of the proportions and nature of
14 112 components added from the slab; such components may change as subduction progresses. To
15 113 unravel the temporal admixtures of mantle and subduction components therefore requires a
16 114 comprehensive elemental and isotopic dataset of volcanics that span the established
17 115 stratigraphic framework of early arc magmatism. This contribution presents new geochemical
18 116 dataset as well as $^{40}\text{Ar}/^{39}\text{Ar}$ ages for samples from the entire volcanic history of the Bonin
19 117 Islands. These data are used to establish the geochemical evolution of early arc magmatism,
20 118 and investigate the processes operating during the establishment of a new subduction zone.
21 119

22 120 **GEOLOGICAL BACKGROUND**

23 121
24 122 The Izu-Bonin arc marks the eastern margin of the Philippine Sea plate and is formed by
25 123 westward subduction of the Pacific plate (Fig. 1a). This arc extends from southern Honshu to
26 124 the south of Ito-Ito Island, and continues further south as the Mariana arc. Izu-Bonin arc has a
27 125 broad volcanic zone extending in an east-west direction and is bounded by the Izu-Ogasawara
28 126 Trench to the east and the Shikoku Basin to the west. Between 25°N and 29°N, there is a
29 127 prominent N-S trending forearc massif called the Bonin Ridge in an area between the
30 128 Quaternary volcanic front and Izu-Ogasawara Trench (Fig. 1a,b). The Bonin Ridge is separated
31 129 from the volcanic front by the Ogasawara Trough, which rifted in the Eocene or Oligocene (Fig.
32 130 1b; Taylor, 1992; Ishizuka *et al.*, 2006a). This preserved the Bonin Ridge as an intact terrain
33 131 without any effects from later overlapping magmatism.
34 132

35 133 **The subaerial Bonin Ridge**

36 134
37 135 Bonin Islands sit atop an uplifted segment of the Bonin Ridge and expose a sequence of the
38 136 early Izu-Bonin arc volcanism (Fig. 2). The islands are geographically divided into 3 groups
39 137 (Fig. 1b): Mukojima Island Group (northern Bonin Islands), Chichijima Island Group (central
40 138 Bonin Islands) and Hahajima Island Group (southern Bonin Islands). The boninitic sequence,
41
42
43
44
45
46
47
48
49
50
51
52
53
54
55
56
57
58
59
60

1
2
3
4
5
6 139 known as the Maruberiwan Formation, is the stratigraphically lowest unit exposed on the Bonin
7 140 islands (Fig. 2). This unit includes boninite, bronzite andesite, dacite and rhyolite (Umino,
8 141 1985; Umino & Nakano, 2007), and is exposed on the Chichijima Island Group as well as the
9 142 Mukojima Island Group. Maruberiwan Formation boninites mostly classify as high-Si boninite
10 143 (Kanayama *et al.*, 2012) and were formed in the Eocene between 46-48 Ma (Cosca *et al.*, 1998;
11 144 Ishizuka *et al.*, 2006a, 2011a). A quartz-bearing dacite-rhyolite sequence (Asahiyama
12 145 Formation; Umino, 1985) unconformably overlies the Maruberiwan Formation, however, no
13 146 significant time gap exists between the Asahiyama Formation and underlying boninitic rocks
14 147 (45.8 Ma; Ishizuka *et al.*, 2011a). The youngest volcanics on the Chichijima Island Group are
15 148 the lavas and clastics of the Mikazukiyama Formation. These high-Mg two-pyroxene andesites
16 149 and low-Si boninites (Kanayama *et al.*, 2012) unconformably overlie the rhyolites of the
17 150 Asahiyama Formation (Fig. 2; 44.3-44.74 Ma).

18 151 Tholeiitic to calcalkaline basaltic to andesitic rocks from Hahajima Island Group are the
19 152 youngest volcanic sequence exposed on any of the Bonin Islands (Fig. 2; Taylor & Nesbitt,
20 153 1995; Ishizuka *et al.*, 2006a; Kanayama *et al.*, 2014; Umino *et al.*, 2016). An $^{40}\text{Ar}/^{39}\text{Ar}$ age of
21 154 44.0 ± 0.3 Ma has been reported for an andesite lava from Hahajima (Ishizuka *et al.*, 2006a).

22 155

23 156 **Submarine section of the Bonin Ridge**

24 157

25 158 A recent investigation of the submarine section east of the Bonin Ridge has expanded the
26 159 forearc stratigraphy to beneath that exposed on the Bonin Islands (Ishizuka *et al.*, 2011a). This
27 160 was found to consist of basalt lava flows and basaltic sheeted dykes, which were named forearc
28 161 basalt (FAB) solely based on their current geographic location (Reagan *et al.*, 2010). $^{40}\text{Ar}/^{39}\text{Ar}$
29 162 dating of these forearc basalts indicate an age between 48 and 52 Ma (Ishizuka *et al.*, 2011a).
30 163 This predates the boninites and implies that the first magmatism following subduction initiation
31 164 was produced at around 52 Ma. Zircon U-Pb ages of gabbro are 51.6 and 51.7 Ma, respectively,
32 165 suggesting that the FAB and gabbros are co-magmatic (Ishizuka *et al.*, 2011a).

33 166 Li *et al.* (2013) reported low-Ca (high-Si) boninite from Hahajima Seamount (ESE of
34 167 Hahajima Island: Fig. 1b) with a $^{40}\text{Ar}/^{39}\text{Ar}$ age of 44 ± 1.4 Ma. They argued that genesis of
35 168 boninite involves melting of subducted volcanoclastic sediments derived from a HIMU
36 169 seamount and Pacific slab as well as depleted Indian MORB-type mantle.

37 170 IODP Exp. 352 drilled in the Bonin forearc and recovered both forearc basalt and boninite at
38 171 different Sites (Reagan *et al.*, 2017, 2019; Shervais *et al.*, 2019). The forearc basalt section
39 172 reconfirmed that FAB magmatism initiated at around 52 Ma (Reagan *et al.*, 2019). Geochemical
40 173 characteristics of the FAB imply that two stages of melting took place to produce FAB magma
41 174 (Shervais *et al.*, 2019). First stage melting is estimated to have occurred in the garnet stability

1
2
3
4
5
6 175 field, probably hundreds of millions of years before subduction initiation (Yogodzinski *et al.*,
7 176 2018). Second stage melting is estimated to be of a larger degree, occurring at higher
8
9 177 temperature and lower pressure (1400-1480°C, 1-2 GPa) compared to that for N-MORB.

10 178 Drilling also revealed that low-Si boninite erupted at 51.3 Ma with a clear slab-derived
11
12 179 signature (Li *et al.*, 2019). Based on these results, Reagan *et al.* (2019) concluded that FAB
13
14 180 magmatism lasted for a short period of around 0.7 Myr. Subsequent supply of a slab-derived
15
16 181 flux initiated boninite magmatism from melting of the depleted mantle residue after FAB
17
18 182 extraction.

183

19 184 **Spatial variation of volcanism**

20 185

21
22 186 Forearc basalts are found on the inner trench wall of the Izu-Ogasawara Trench, i.e., the
23
24 187 easternmost volcanic sequence in this area. A high-Si boninitic sequence younger than 48 Ma
25
26 188 occurs on the shallower slope of the inner trench wall, i.e., west of the forearc basalts and on
27
28 189 the Bonin Islands. Post-44 Ma tholeiitic and calcalkaline lavas are exposed along the western
29
30 190 escarpment of the Bonin Ridge, just west of the Bonin Islands where boninites occur, as well
31
32 191 as on the Hahajima Islands (Ishizuka *et al.*, 2006a). Thus, based on these observations, the locus
33
34 192 of volcanism appears to have moved westward, i.e. away from the trench, with time (Ishizuka
35
36 193 *et al.*, 2011a). This may be related to the progressive establishment of subduction and a well-
37
38 194 defined mantle wedge (e.g., Stern, 2004; Ishizuka *et al.*, 2006a, 2011a). Extension of the
39
40 195 overriding plate at subduction initiation might have controlled the location of the forearc
41
42 196 basaltic volcanism (e.g., Stern & Bloomer, 1992; Hall *et al.*, 2003), and then cooling of the
43
44 197 mantle wedge by the sinking slab, counter flow of asthenospheric mantle, and initiation of slab
45
46 198 dehydration/melting all could have affected the focus of volcanism after 48 Ma (e.g., Ishizuka
47
48 199 *et al.*, 2006a).

200

201 **SAMPLES STUDIED**

202

203 Samples used in this study were mainly collected during geological mapping campaigns on the
204
205 204 Bonin Islands (Umino & Nakano, 2007; Umino *et al.*, 2009, 2015). They are representative of
206
207 205 all subaerially exposed volcanics, and cover the entire age-range of magmatism exposed on the
208
209 206 Bonin Islands (Fig. 2). High-Si boninite series rocks (Kanayama *et al.*, 2012) were collected
210
211 207 from the Mukojima Island and Chichijima Island Groups, reported in this contribution as
212
213 208 Mukojima and Chichijima groups, respectively. Transitional high-Mg cpx-opx andesites and
214
215 209 low-Si boninites (Kanayama *et al.*, 2012) of the Mikazukiyama Formation were collected from
216
217 210 Chichijima and Otoutojima, and described as Mikazukiyama group. Other younger basaltic to
218
219 211
220

211 andesitic rocks were collected from the Hahajima Island Group (reported as Hahajima group).
212 Exact sample localities are listed in Tables S1-S5. For some of the samples from Mukojima,
213 Chichijima and Hahajima Island Groups, whole rock chemical compositions have been
214 published in Taylor *et al.* (1994), Kanayama *et al.* (2012, 2014) and Ishizuka *et al.* (2014b).

215 The samples used for analyses were selected from the much larger number of samples
216 collected during the mapping campaign. Sample selection was mainly based on microscopic
217 observation of thin sections and, in some cases, stereomicroscopic observation of rocks. Criteria
218 for sample selection were; 1) The sample should mostly retain fresh groundmass, 2) Most of
219 the phenocrysts are fresh, 3) Free from secondary mineral crystallisation (e.g., zeolites, opal)
220 inside vesicles.

221 Specifically for $^{40}\text{Ar}/^{39}\text{Ar}$ dating, only high-Si boninites, which retain pristine glassy
222 groundmass, were chosen. For samples from the Mikazukiyama group and Hahajima group,
223 those with relatively crystalline groundmass composed of mainly plagioclase and pyroxene
224 with only minor amounts of fresh interstitial glass were selected.

226 ANALYTICAL PROCEDURES

227 Whole rock chemistry

229 About 20 g of rock chips were ultrasonically cleaned with distilled water, and then crushed with
230 an iron pestle and pulverised using an agate mortar. Whole rock major elements were analysed
231 on glass beads, prepared by fusing 1:10 mixtures of 0.5 g subsamples and lithium tetraborate.
232 The glass beads were analysed using a Panalytical Axios XRF spectrometer at the Geological
233 Survey of Japan/AIST. External uncertainty and accuracy are generally <2% (2.s.d), but Na
234 could have as much as ~7% analytical uncertainty. The data for each element are in agreement
235 with accepted values and uncertainties of international standards (Table S1).

236 The rare-earth elements (REE), V, Cr, Ni, Rb, Sr, Y, Zr, Nb, Cs, Ba, Hf, Ta, Pb, Th and U
237 concentrations were analysed by ICP-MS on a VG Platform instrument and Agilent 7900, both
238 at the Geological Survey of Japan/AIST. About 100 mg of powder from each sample was
239 dissolved in a HF-HNO₃ mixture (5:1) using screw-top Teflon beakers. After evaporation to
240 dryness, the residues were re-dissolved with 2% HNO₃ prior to analysis. In and Re were used
241 as internal standards, while JB2 with a similar level of dilution to the samples was used as an
242 external standard during ICP-MS measurements. Instrument calibration was performed using
243 5-6 calibration solutions made from international rock standard materials (including BIR-1,
244 BCR-1, AGV-1, JB1a, BEN). Reproducibility is generally better than ±4% (RSD) for the REE,
245 and better than ±6% (RSD) for other elements except those with very low concentration and Ni
246 (see BHVO2 analysis in Table S1). Detection limits vary from element to element, but for

1
2
3
4
5
6 247 elements with low concentrations, such as REE and Ta, limits typically fall within a range from
7 248 0.2 to 2 pg g⁻¹.

8
9 249

10 250 **Radiogenic isotopic composition**

11 251

12 252 Isotopic compositions of Sr, Nd, and Pb were determined on 500 mg of hand-picked 0.5–1mm
13 253 rock chips. The chips were leached in 6M HCl at 140°C for 20-30 minutes prior to dissolution
14 254 in HF-HNO₃. Sr, Nd and Pb isotope ratios were measured on a nine-collector VG Sector 54
15 255 mass spectrometer. Sr was isolated using Sr resin (Eichrom Industries, Illinois, USA). For Nd
16 256 isotopic analysis, the REE were initially separated by cation exchange, before isolating Nd on
17 257 Ln resin (Eichrom Industries, Illinois, USA) columns. Procedural Sr and Nd blanks were
18 258 considered negligible relative to the amount of sample analysed. Sr and Nd isotopic
19 259 compositions were determined as the average of 150 ratios by measuring ion beam intensities
20 260 in multi-dynamic collection mode. Isotope ratios were normalised to ⁸⁶Sr/⁸⁸Sr = 0.1194 and
21 261 ¹⁴⁶Nd/¹⁴⁴Nd = 0.7219. Measured values for NBS SRM-987 and JNdi-1 (Tanaka *et al.*, 2000)
22 262 were ⁸⁷Sr/⁸⁶Sr = 0.710278 ± 19 (2 s.d., n = 33) and ¹⁴³Nd/¹⁴⁴Nd = 0.512104 ± 10 (2 s.d., n = 38)
23 263 during the measurement period. All ⁸⁷Sr/⁸⁶Sr ratios were normalised to NBS SRM-987 ⁸⁷Sr/⁸⁶Sr
24 264 = 0.710248 (Thirlwall, 1991), and ¹⁴³Nd/¹⁴⁴Nd ratios were normalised to JNdi-1 = 0.512115
25 265 (Tanaka *et al.*, 2000) as measured during the same analytical session.

26
27 266 The Pb isotopic compositions were determined at the Geological Survey of Japan/AIST and
28 267 University of Southampton, UK. Average isotope ratio data from both laboratories was found
29 268 to be within ~1 s.d., and were within similar levels of uncertainty of the poly-spike SRM 981
30 269 values of Taylor *et al.*, (2015). Consequently data presented are not internally adjusted or
31 270 normalised. At the Geological Survey of Japan/AIST, Pb separation was achieved using AG1-
32 271 X8 200-400 mesh anion exchange resin. Procedural Pb blanks were <30pg, and considered
33 272 negligible relative to the amount of sample analysed. Pb isotopic measurements were made in
34 273 multi-dynamic collection mode using the double spike technique (Southampton-Brest-Lead
35 274 207-204 spike SBL74: (Ishizuka *et al.*, 2003; Taylor *et al.*, 2015)). Natural (unspiked)
36 275 measurements were made on 60-70 % of collected Pb, giving ²⁰⁸Pb beam intensities of 2.5-3 ×
37 276 10⁻¹¹A. Fractionation-corrected Pb isotopic compositions and internal errors were obtained by
38 277 a closed-form linear double-spike deconvolution (Johnson & Beard, 1999). The reproducibility
39 278 of Pb isotopic measurements (external error: 2 s.d.) by double spike is <200 ppm for all
40 279 ^{20x}Pb/²⁰⁴Pb ratios. Measured values for NBS SRM-981 during the measurement period were
41
42
43
44
45
46
47
48
49
50
51
52
53
54
55
56
57
58
59
60

280 $^{206}\text{Pb}/^{204}\text{Pb}=16.9407 \pm 0.0039$, $^{207}\text{Pb}/^{204}\text{Pb}=15.5010 \pm 0.0050$, and $^{208}\text{Pb}/^{204}\text{Pb}=36.724 \pm 0.012$
281 (2 s.d., n = 21).

282 At the University of Southampton, rocks were prepared for Pb isotope analysis by initially
283 crushing inside a plastic envelope using a non-torque press. Crushed material was then
284 separated to 0.5-1.0 mm using a Teflon sieve set. This fraction was repeatedly cleaned with in
285 ultra-pure water in an ultra-sonic bath. Cleaned rock-chips were then picked during microscopic
286 examination. Samples were leached for 30-40 min in 4M HCl at 200°C prior to Pb separation
287 using HBr-HCl anion exchange columns. Lead isotope ratios were measured by a Thermo
288 Neptune MC-ICP-MS at the University of Southampton UK, using a double spike run of each
289 sample to correct for instrumental mass fractionation. The ^{207}Pb - ^{204}Pb SBL74 spike was added
290 such that $^{204}\text{Pb}_{\text{sample}}/^{204}\text{Pb}_{\text{spike}}$ was 0.09 ± 0.03 . Procedural blanks range between 50-100 pg Pb.
291 NBS SRM 981 values achieved during the measurement period were $^{206}\text{Pb}/^{204}\text{Pb} = 16.9406$
292 ± 0.0030 , $^{207}\text{Pb}/^{204}\text{Pb} = 15.4980 \pm 0.0030$, $^{208}\text{Pb}/^{204}\text{Pb} = 36.7188 \pm 0.0086$ (2s.d.; n = 17).

293 The Hf isotope ratios were measured on a Thermo Neptune MC-ICP-MS at the University of
294 Southampton, UK. Hf isotope ratios were monitored and corrected for mass fractionation using
295 $^{179}\text{Hf}/^{177}\text{Hf} = 0.7325$ and for interferences using the values reported in Chu *et al.* (2002). Hf
296 isotopes are reported relative to $^{176}\text{Hf}/^{177}\text{Hf}$ of JMC 475 of 0.282158. Repeated JMC 475
297 measurements during the measurement period gave $^{176}\text{Hf}/^{177}\text{Hf} = 0.282161 \pm 0.000010$ (2s.d.;
298 n = 26).

300 $^{40}\text{Ar}/^{39}\text{Ar}$ dating

302 Ages of the fresh volcanic rocks were determined using the $^{40}\text{Ar}/^{39}\text{Ar}$ dating facility at the
303 Geological Survey of Japan/AIST. Details of the procedures are reported in Ishizuka *et al.*
304 (2009, 2018). 20-25 mg of phenocryst-free groundmass, crushed and sieved to 250 – 500 μm
305 in size, was analysed using a stepwise heating procedure. The samples were treated in 6N HCl
306 for 30 minutes at 95°C with stirring to remove any alteration products (clays and carbonates)
307 present in interstitial spaces. After this treatment, samples were examined under a microscope.
308 Sample irradiation was done at the JRR3 and JRR4 reactors for 24 hours except for the sample
309 06062604C irradiated at the CLICIT facility of the Oregon State University TRIGA reactor for
310 4 hours. Sanidine separated from the Fish Canyon Tuff (FC3) was used as flux monitor and
311 assigned an age of 27.5 Ma, which has been determined against the primary standard for our
312 K-Ar laboratory, Sori biotite, the age of which is 91.2 Ma (Uchiumi & Shibata, 1980).

313 A CO₂ laser heating system (NEWWAVE MIR10-30) was used in continuous wave mode

1
2
3
4
5
6 314 for sample heating. A faceted lens was used to obtain a 3.2 mm-diameter beam with
7 315 homogenous energy distribution to ensure uniform heating of the samples during stepwise
8
9 316 heating analysis. Argon isotopes were measured on a VG Isotech VG3600 noble gas mass
10 317 spectrometer fitted with a BALZERS electron multiplier except for sample 06062604C, which
11 318 was measured on an IsotopX NGX noble gas mass spectrometer fitted with a Hamamatsu
12 319 Photonics R4146 secondary electron multiplier in a peak-jumping mode.

13
14
15 320 Correction for interfering isotopes was achieved by analyses of CaF_2 and KFeSiO_4 glasses
16 321 irradiated with the samples. The blank of the system including the mass spectrometer and the
17 322 extraction line was 7.5×10^{-14} ml STP for ^{36}Ar , 2.5×10^{-13} ml STP for ^{37}Ar , 2.5×10^{-13} ml STP
18 323 for ^{38}Ar , 1.0×10^{-12} ml STP for ^{39}Ar and 2.5×10^{-12} ml STP for ^{40}Ar with the VG3600
19 324 instrument, and 2.9×10^{-14} ml STP for ^{36}Ar , 1.4×10^{-13} ml STP for ^{37}Ar , 1.0×10^{-14} ml STP for
20 325 ^{38}Ar , 1.2×10^{-14} ml STP for ^{39}Ar and 1.9×10^{-12} ml STP for ^{40}Ar with the NGX mass
21 326 spectrometer. Blank analyses were done every 2 or 3 step analyses. All errors for $^{40}\text{Ar}/^{39}\text{Ar}$
22 327 results are reported at one standard deviation. Errors for ages include analytical uncertainties
23 328 for Ar isotope analysis, correction for interfering isotopes, and J value estimation. An error of
24 329 0.5 % was assigned to J values as a pooled estimate during the course of this study. Results of
25 330 Ar isotopic analyses and correction factors for interfering isotopes are presented in the
26 331 supplementary data (Table S6).

27
28
29
30
31
32
33 332 Plateau ages were calculated as weighted means of ages of plateau-forming steps, where each
34 333 age was weighted by the inverse of its variance. The age plateaus were determined following
35 334 the definition by Fleck *et al.* (1977). Inverse isochrons were calculated using York's least-
36 335 squares fit, which accommodates errors in both ratios and correlations of errors (York, 1969).

37
38
39 336

40 337 **RESULTS**

41 338 $^{40}\text{Ar}/^{39}\text{Ar}$ ages

42 339

43
44
45 340 Six samples from the Hahajima group and one low-Si boninite from the Mikazukiyama group
46 341 were dated by $^{40}\text{Ar}/^{39}\text{Ar}$ (Table 1; Fig. 3). Three samples from Hahajima gave ages between
47 342 40.2 and 45.28 Ma. For one sample (10093001-1), $^{36}\text{Ar}/^{40}\text{Ar}$ intercept of an inverse isochron
48 343 plot does not agree with the atmospheric ratio within 2σ error. However, this is because the data
49 344 points form a tight cluster near the radiogenic end of the plot, and the $^{36}\text{Ar}/^{40}\text{Ar}$ intercept is not
50 345 well constrained. The weighted average of ages of 13 steps can be regarded as a reliable
51 346 eruption age for this sample. The ages from the Hahajima Island are stratigraphically consistent
52 347 (Umino *et al.*, 2016), i.e., two older samples (42.66 and 45.28 Ma) are from the lowermost
53 348 Higashidai Formation and the youngest age (40.2 Ma) is from the uppermost Sekimon
54 349 Formation (Fig. 2). Three Hahajima group samples from other islands of the Hahajima Island
55
56
57
58
59
60

1
2
3
4
5
6 350 Group gave ages between 38.4 and 44.6 Ma, which are overlapping or slightly younger than
7 351 the ages from the Hahajima Island. Two samples (05122110 and 10092707-1) do not satisfy
8 352 the definition of “age plateau” in a strict sense. For these samples, higher temperature steps
9 353 which show decreasing ages as applied heating temperature increases appears to have been
10 354 affected by recoil, but lower to middle temperature steps show constant ages and seem to be
11 355 free from that effect. The weighted averages of the consecutive steps giving identical ages are
12 356 adopted as best estimate for the eruption ages, which are consistent with regional stratigraphy.

13 357 A low-Si boninite of the Mikazukiyama group from the Otoutojima island of the Chichijima
14 358 Island Group gave an age of 45.16 Ma, which is identical to the ages of cpx-opx andesites from
15 359 the same formation within the 2σ uncertainty (Ishizuka *et al.*, 2006a, 2011a).

16 360

17 361 **Major element compositions**

18 362

19 363 Volcanics from the Bonin Islands show mainly andesitic/intermediate SiO_2 contents with some
20 364 minor differentiated rocks including dacite and rhyolite, with basaltic rocks only present in the
21 365 Hahajima group. Each volcanic group defines a distinct compositional range and trend on major
22 366 element plots (Fig. 4). For example, taken at 8 wt% MgO, boninites from Mukojima and
23 367 Chichijima have the highest SiO_2 (58-60 wt%), Hahajima group the lowest SiO_2 (50-55 wt%),
24 368 with the cpx-opx andesites from the Mikazukiyama group at an intermediate level (Fig. 2, 4a).
25 369 Mukojima and Chichijima boninites can be categorized as high-Si boninite (Kanayama *et al.*,
26 370 2012).

27 371 In the Mikazukiyama group, boninites are the low-Si variety, whereas the cpx-opx andesites
28 372 in this group have higher SiO_2 and lower MgO than the boninites (Fig. 4a). Boninite series
29 373 rocks are absent in the Hahajima group, and instead both tholeiitic and calcalkaline basalts to
30 374 andesites are present (Fig. 4b).

31 375 TiO_2 and CaO also show distinct trends among the different units. CaO and TiO_2 at a given
32 376 MgO are lowest in the high-Si boninites, moderate in the low-Si boninites and cpx-opx
33 377 pyroxene andesites in the Mikazukiyama group, and highest in the Hahajima group (Fig. 2,
34 378 4c,d).

35 379

36 380 **Trace element compositions**

37 381

38 382 Trace element ratios associated with fluid-mobile element enrichment are distinct among the
39 383 different volcanic units. All volcanics from the Bonin Islands show significantly lower Ce/Pb

40 384

1
2
3
4
5
6 384 relative to N-MORB (24.3: Gale et al., 2013: Fig. 5a) and most of the OIB (10-40: Willbold
7 385 and Stracke, 2006). High-Si boninites from the Chichijima and Mukojima groups show the
8 386 lowest Ce/Pb, while the Hahajima group shows the highest (Fig. 5a). Mikazukiyama group
9 387 shows slightly higher Ce/Pb than the high-Si boninites except for highly differentiated samples,
10 388 which have Ce/Pb >10, and among the Mikazukiyama group, cpx-opx andesites generally have
11 389 lower Ce/Pb (1.5-3) than low-Si boninite (3-11). Other fluid-mobile elements such as Ba show
12 390 a similar variation in enrichment among the different volcanic units. For example, volcanics
13 391 from the Bonin Islands show significantly higher Ba/Nb relative to N-MORB (around 10: Gale
14 392 et al., 2013) and comparable or higher than OIB (4 -25: Willbold and Stracke, 2006). Ba/Nb
15 393 ratios are the highest for the high-Si boninites (30-130: Fig. 5b), while the Hahajima group
16 394 shows the lowest Ba/Nb (10-50). The Mikazukiyama group again shows intermediate ratios
17 395 between the high-Si boninites and the Hahajima group (mostly 20-90), and cpx-opx andesites
18 396 show higher Ba/Nb than low-Si boninites.

19 397 Th enrichments yield different characteristics compared to those of the fluid-mobile elements.
20 398 Th/Ce or Th/Nb (not shown) ratios are relatively high for the high-Si boninites and the
21 399 Mikazukiyama group, and significantly higher than N-MORB (0.02 for Th/Ce, and 0.07 for
22 400 Th/Nb: Gale et al., 2013), and lower in the Hahajima group (Fig. 5c), comparable or slightly
23 401 higher than N-MORB. Some of the cpx-opx andesites from the Mikazukiyama group show
24 402 particularly high Th/Ce and Th/Nb.

25 403 Light rare earth element (LREE) ratios such as La/Sm also show differences between the
26 404 different groups, i.e., the high-Si boninites show the highest La/Sm, higher than N-MORB (1.2:
27 405 Gale et al., 2013), and the Hahajima Group further extends to the lowest La/Sm ratios among
28 406 the Bonin Islands volcanics, as low as comparable to N-MORB, while La/Sm ratios in the
29 407 Mikazukiyama group overlap with those of the high-Si boninites (Fig. 5d).

30 408 Middle to heavy rare earth element ratios such as Dy/Yb are lowest in high-Si boninites, and
31 409 the Hahajima group show the highest ratios, with intermediate ratios for both cpx-opx andesites
32 410 and low-Si boninites from the Mikazukiyama group (Fig. 5e).

33 411 High-Si boninites have lower Sm/Zr than other volcanics from the Bonin Islands and N-
34 412 MORB (0.034: Gale et al., 2013). Low-Si boninites of the Mikazukiyama group show
35 413 comparable ratios to the highest ratios amongst the high-Si boninites. The Hahajima group
36 414 shows decreasing Sm/Zr with increasing Sm, while low-Si boninite and cpx-opx andesite of the
37 415 Mikazukiyama group have increasing Sm/Zr with increasing Sm (Fig. 5f).

38 416 Nb/Zr ratios of Bonin Island volcanics are generally lower than N-MORB (0.036). In the

1
2
3
4
5
6 417 high-Si boninites this ratio is generally 0.012-0.02, with some Mukojima group boninites
7 418 extending this to 0.035. Most of the low-Si boninites from the Mikazukiyama group have higher
8 419 Nb/Zr ratios (0.02-0.035) than the high-Si boninites from Chichijima group, and overlap with
9 420 those of the Hahajima group (Fig. 5g).
10
11
12
13

421 422 **Radiogenic isotopes**

423
424 A clear feature of the Pb isotopes from the Chichijima and Mukojima high-Si boninites are the
425 positive trends extending from $\Delta^{207}\text{Pb}/^{204}\text{Pb}$ \sim 2 to 7 and $\Delta^{208}\text{Pb}/^{204}\text{Pb}$ \sim 15 to 30, while
426 $^{206}\text{Pb}/^{204}\text{Pb}$ varies from \sim 18.5 to 18.7 ($\Delta^{207}\text{Pb}/^{204}\text{Pb}$ and $\Delta^{208}\text{Pb}/^{204}\text{Pb}$ are vertical deviation in
427 $^{207}\text{Pb}/^{204}\text{Pb}$ and $^{208}\text{Pb}/^{204}\text{Pb}$ from the Northern Hemisphere Reference Line (NHRL: Hart, 1984;
428 Zindler and Hart, 1986), Fig. 6a and b). In $^{207}\text{Pb}/^{204}\text{Pb}$ - $\Delta^{207}\text{Pb}/^{204}\text{Pb}$ (Fig. 6c), these groups form
429 strong positive correlations extending to high $^{207}\text{Pb}/^{204}\text{Pb}$ (15.6). In each of these projections,
430 samples from the Mukojima group form a discrete, sub-parallel trend to the Chichijima group,
431 but are offset to \sim 0.1 higher $^{206}\text{Pb}/^{204}\text{Pb}$. In contrast, the Mikazukiyama low-Si boninites form
432 a trend extending to high $^{206}\text{Pb}/^{204}\text{Pb}$ (19.5), low $\Delta^{208}\text{Pb}/^{204}\text{Pb}$ (-30) and constant $\Delta^{207}\text{Pb}/^{204}\text{Pb}$
433 (\sim -1.5). Mikazukiyama cpx-opx andesites form a short, steep trend close to the NHRL, but with
434 $^{206}\text{Pb}/^{204}\text{Pb}$ decreasing with increasing ΔPb . This trend is coincident with the upper “off-axis”
435 boninites from IODP Exp. 352 (Fig. 6 a-c). The Hahajima group forms a compact group with
436 similar $^{206}\text{Pb}/^{204}\text{Pb}$ and $\Delta^{207}\text{Pb}/^{204}\text{Pb}$ to Pacific MORB, but with $\Delta^{208}\text{Pb}/^{204}\text{Pb}$ elevated to \sim 12.
437 Overall, the Hahajima group forms a diffuse trend to lower Δ -values with higher $^{206}\text{Pb}/^{204}\text{Pb}$, in
438 a similar fashion to the Mikazukiyama low-Si boninites.
439 High-Si boninites show the highest $^{87}\text{Sr}/^{86}\text{Sr}$ and lowest $^{143}\text{Nd}/^{144}\text{Nd}$ ratios among the early arc
440 volcanics from the Bonin Islands. (Fig. 6d). The Hahajima group shows the lowest $^{87}\text{Sr}/^{86}\text{Sr}$
441 and highest $^{143}\text{Nd}/^{144}\text{Nd}$, while cpx-opx andesites and low-Si boninites of the Mikazukiyama
442 group have intermediate ratios between high-Si boninites and the Hahajima group. Figure 6e
443 shows that high-Si boninites from the Chichijima and Mukojima groups have a wide range of
444 $^{143}\text{Nd}/^{144}\text{Nd}$ (ϵNd \sim 2.5-7.5) at constant $^{206}\text{Pb}/^{204}\text{Pb}$ (18.65 ± 0.1). This compares to Hahajima
445 and Mikazukiyama, which have relatively invariant ϵNd \sim 6.5-8.5; regardless of their spread in
446 $^{206}\text{Pb}/^{204}\text{Pb}$ (18.4-19.5). Despite the spread of ϵNd on Chichijima there is little corresponding
447 change in ϵHf (12.1-13.5), which contrasts with Hahajima and Mikazukiyama, where ϵHf is
448 dispersed in the range 11.3-17.5 (Fig. 6f).
449

450 **DISCUSSION**

451 **Volcanism moves away from the trench**

452
453 New dating results presented in this study as well as those from IODP Exp. 352 (Reagan *et al.*,
454 2019) support the earlier interpretations regarding the temporal variation of early arc
455 magmatism (Ishizuka *et al.*, 2006a; 2011a). Following the trench-proximal FAB at 51-52 Ma,
456 magmatism progresses westwards across the arc. Reagan *et al.* (2019) showed that boninites
457 drilled at U1439 of IODP Exp.352 on the trench slope east of the Mukojima Islands are 50.33-
458 51.27 Ma; ~2 Myr older than subaerially-exposed boninites from the Bonin Islands. This result
459 indicates that boninite magmatism started with the low-Si boninite, and then high-Si boninites
460 at around 51 Ma within c. 10 km from the FAB site (Reagan *et al.*, 2019). Subsequently, the
461 location of high-Si boninite magmatism migrated westward, i.e., toward the present day Bonin
462 Islands, and this magmatism lasted around 4 million years until 46 Ma, to be followed by dacite
463 and rhyolite magmatism of the Asahiyama Formation at 45-46 Ma (Table 1, Ishizuka *et al.*,
464 2006a; 2011a). The Asahiyama volcanics can be viewed as a product of crystal fractionation of
465 boninite magma (Taylor *et al.*, 1994). Ages of the boninites thus imply that the locus of boninite
466 magmatism migrated away from the trench with time.

467 Low-Si boninite and cpx-opx andesites of the Mikazukiyama group erupted at around 45 Ma,
468 and lasted for less than a million years.

469 The youngest magmatism (38.4-45 Ma) occurred in the Hahajima group in the southern Bonin
470 Islands, and along the western escarpment of the Bonin Ridge to the west off the Mukojima and
471 Chichijima Islands (Ishizuka *et al.*, 2006a). Furthermore, dredge sampling to the east of
472 Hahajima Island (D30 of KH07-2 cruise; Fig. 1b) recovered boninites, confirming the east-west
473 spatial sequence along this 350 km long segment of the arc. Dating results support for the
474 interpretation that following subduction initiation, magmatism migrated about 80 km away
475 from the trench with time, over a period of 7-8 million years.

476

477 **Changes in slab input**

478

479 Isotopic variations amongst the Bonin volcanics could have been generated by a number of
480 potential sources. These are:

481 1) Pre-existing crust

482 2) Subducted pelagic or volcanoclastic sediment

1
2
3
4
5
6 483 3) Subducted igneous ocean crust/lithosphere

7
8 484 4) The supra-subduction mantle (mantle wedge)

9
10 485 These components may contribute to the composition of the system either via a fluid, a melt
11 or as a solid/melted assimilant. In the current Izu-Bonin-Mariana arc, there are good constraints
12 486 on the isotopic composition and elemental abundances of most of these components (e.g., Hauff
13 487 *et al.*, 2003; Plank *et al.*, 2007; Durkin *et al.*, *in press*). In general terms at least, the recently
14 488 subducted and current supra-subduction material are likely to be similar to those of the Eocene.
15 489 As such, we assume that these compositions can be used to assess inputs to the Bonin Island
16 490 volcanism. Recent drilling through the Eocene-Oligocene Izu-Bonin-Mariana rear-arc
17 491 confirmed that pre-existing crust is equivalent to Indian MORB (i.e. Philippine Sea MORB:
18 492 Hickey-Vargas *et al.*, 1995) ocean crust (Ishizuka *et al.*, 2018; Hickey-Vargas *et al.*, 2018;
19 493 Yogodzinski *et al.*, 2018). As such, this pre-existing crust has similar Indian isotopic
20 494 characteristics to the forearc basalts, indicating the mantle wedge was characterised by
21 495 $\Delta^{208}\text{Pb}/^{204}\text{Pb} \sim 40$ and $\Delta^{207}\text{Pb}/^{204}\text{Pb}$ 0-3.
22 496

23 497 Sedimentary components on the current Pacific plate span the age range of Bonin Island
24 498 volcanism. These comprise pelagic sediments and seamount-derived volcanoclastic sediments,
25 499 which are variably distributed along the length of the current arc (Kelley *et al.*, 2003; Plank *et*
26 500 *al.*, 2007; Straub *et al.*, 2009: Fig. 6). Some latitudinal variation is present in the sedimentary
27 501 material, for example between ODP Sites 1149 and 801 of the Izu-Bonin and Mariana arcs,
28 502 respectively (Plank & Langmuir, 1998; Plank *et al.*, 2007: Fig. 6). This may be reflected in the
29 503 isotopic variation in Pb isotopes along the active Izu-Bonin-Mariana arc (Taylor & Nesbitt,
30 504 1998; Ishizuka *et al.*, 2006b, 2007).

31 505 Subducted altered ocean crust in the current system is Pacific MORB with seamounts of
32 506 HIMU or EM composition (Koppers *et al.*, 1998, 2003; Durkin *et al.*, *in press*). It is possible
33 507 that Indian MORB compositions were present on the Pacific Plate in the Eocene, but have
34 508 subsequently been consumed by subduction (Straub *et al.*, 2009). Alteration by syn-magmatic
35 509 hydrothermal processes and by seawater interaction may have modified primary magmatic
36 510 compositions of volcanoclastic material and oceanic crust. Such processes generally increase U
37 511 relative to Th and Pb which, as shown in Fig. 6 a-c and e, results in lower $\Delta^{207}\text{Pb}/^{204}\text{Pb}$ and
38 512 $\Delta^{208}\text{Pb}/^{204}\text{Pb}$ (often highly negative) with higher $^{206}\text{Pb}/^{204}\text{Pb}$ (Hauff *et al.*, 2003; Straub *et al.*,
39 513 2009; Li *et al.*, 2019).

40 514 Positive correlations between fluid-mobile element enrichment and isotopes, such as Ba and
41
42
43
44
45
46
47
48
49
50
51
52
53
54
55
56
57
58
59
60

1
2
3
4
5
6 515 $^{87}\text{Sr}/^{86}\text{Sr}$ and $^{206}\text{Pb}/^{204}\text{Pb}$, are indicative of radiogenic components added to a Indian MORB-
7 516 type mantle (Fig. 7a). This component has been interpreted as slab-derived material added to
8 517 the source of boninite magma from the subducting Pacific plate (e.g., Taylor *et al.*, 1994;
9 518 Ishizuka *et al.*, 2006a, 2011a; Li *et al.*, 2019).

10
11
12 519 Pb isotope variation within high-Si boninites from the Chichijima and Mukojima groups
13 520 defines a strong alignment between Pacific pelagic sediment with high ΔPb and Pacific MORB
14 521 or its altered, subducting equivalent with low ΔPb (Fig. 6a-c). The lack of a trajectory to high
15 522 $\Delta^{208}\text{Pb}/^{204}\text{Pb}$ with low $^{206}\text{Pb}/^{204}\text{Pb}$ excludes significant Pb derived from the Indian MORB
16 523 mantle wedge ($\Delta^{208}\text{Pb}/^{204}\text{Pb} > 30$). Notably, Chichijima and Mukojima boninites have Ce/Pb
17 524 < 2 regardless of their Pb isotope ratio (Fig. 7b). This implies that the components that mixed to
18 525 form the Pb isotope trends must also have similarly low Ce/Pb. Indeed, they have significantly
19 526 lower Ce/Pb than subducting Pacific crust or Pacific pelagic sediment. This low Ce/Pb is likely
20 527 a characteristic of fluid released from the subducted crust, which derives its Pb from interaction
21 528 with variable proportions of MORB and sediment. As this Pb-rich fluid was introduced into an
22 529 effectively Pb-free depleted mantle wedge, essentially the entire Pb inventory of the resulting
23 530 partial melts was slab-derived.

24
25
26 531 Correlations between ϵNd , $^{206}\text{Pb}/^{204}\text{Pb}$ and ϵHf for the high-Si boninites from the Chichijima
27 532 and Mukojima groups (Fig. 6e, f) are also indicative of pelagic sediment-Pacific MORB
28 533 interaction. However, the addition of Nd and Hf via subduction implies the carrier may have
29 534 the characteristics of a melt or supercritical fluid rather than a simple aqueous fluid (e.g.,
30 535 Woodhead *et al.*, 2001). This implication is further supported by a negative correlation between
31 536 $^{143}\text{Nd}/^{144}\text{Nd}$ and Th/Ce or La/Sm (Fig. 7c,d).

32
33
34 537 Taylor *et al.* (1994) proposed that the distinctively low Sm/Zr of Chichijima boninites (0.02
35 538 compared to ~ 0.035 for MORB) resulted from slab melting in the presence of residual
36 539 amphibole, but not by crystal fractionation of amphibole. This interpretation appears to be
37 540 applicable to all the high-Si boninites from the Chichijima and Mukojima groups (Fig. 5f).
38 541 Sm/Zr variation of the Hahajima group, however, seems to be compatible with (cryptic) crystal
39 542 fractionation of amphibole, as seen in mature volcanic arcs (e.g., Davidson *et al.*, 2007), which
40 543 consistently explains Sm/Zr variation with Sm content and also decreasing Dy/Yb with
41 544 increasing SiO_2 (Fig. 5e, f).

42
43
44 545 After activity of Chichijima and Mukojima high-Si boninite magmatism, volcanism at 44-45
45 546 Ma became transitional between boninitic and tholeiitic/calc-alkaline. These eruptives are
46 547 represented by the low-Si boninites and cpx-opx andesites of the Mikazukiyama group. This
47
48
49
50
51
52
53
54
55
56
57
58
59
60

1
2
3
4
5
6 548 switch in magmatism was accompanied by a sharp change in the characteristics of the
7 549 subduction components. Neither of the Mikazukiyama magma types show any significant
8
9 550 indication of a Pb isotope vector towards pelagic sediment. Instead these volcanics trend to
10
11 551 negative $\Delta^{208}\text{Pb}/^{204}\text{Pb}$ and high $^{206}\text{Pb}/^{204}\text{Pb}$ (18.8 – 19.5) compositions. Other characteristics,
12
13 552 such as lower Th/Ce and $^{87}\text{Sr}/^{86}\text{Sr}$ combined with higher Ce/Pb and $^{143}\text{Nd}/^{144}\text{Nd}$ (Fig. 6d, 7b,c)
14
15 553 are also concordant with a significantly smaller pelagic contribution. The overall implication
16
17 554 of this is that, in the central and southern Bonin islands at least, there was a change in the
18
19 555 material released from the slab at around 45 Ma. It is also possible that physical conditions in
20
21 556 the slab changed at the same time. This, in turn, may change the properties of the slab flux (e.g.,
22
23 557 hydrous fluid, siliceous melt, supercritical fluid) and consequently influence the trace element
24
25 558 concentrations in the slab component (e.g., Kessel *et al.*, 2005).

26 559 A possible candidate for a slab-derived component with high $^{206}\text{Pb}/^{204}\text{Pb}$ and low ΔPb is
27
28 560 volcanoclastic material originating from HIMU oceanic islands on the subducting Pacific Plate
29
30 561 (Koppers *et al.*, 1998, 2003; Ishizuka *et al.*, 2007). Since HIMU seamounts in the modern
31
32 562 Western Pacific are as old as 100-120 Ma (Koppers *et al.*, 2003), it is reasonable to assume that
33
34 563 such volcanoclastics were present on the newly subducting Pacific Plate at 45 Ma. Contribution
35
36 564 of this volcanoclastic material instead of pelagic sediment is consistent with lower $^{87}\text{Sr}/^{86}\text{Sr}$ and
37
38 565 higher $^{143}\text{Nd}/^{144}\text{Nd}$ ($\epsilon\text{Nd} \sim -6$) in Mikazukiyama compared to the earlier high-Si boninites. Of
39
40 566 the two groups within Mikazukiyama, the low-Si boninites have higher Nb/Zr, ΔNb (ΔNb is
41
42 567 defined as $\Delta\text{Nb} = 1.74 + \log(\text{Nb}/\text{Y}) - 1.92\log(\text{Zr}/\text{Y})$ to express deficiency or excess of Nb
43
44 568 relative to the OIB compositions: Fitton *et al.* (1997)) and $^{206}\text{Pb}/^{204}\text{Pb}$, suggesting they may
45
46 569 have a larger contribution from the HIMU volcanoclastics relative to the cpx-opx andesites (Fig.
47
48 570 8).

49 571
50 572 A further change in the subduction system occurred with the Hahajima group, which followed
51
52 573 the Mikazukiyama group. Hahajima samples shift back to lower $^{206}\text{Pb}/^{204}\text{Pb}$ (18.5) at
53
54 574 $\Delta^{207}\text{Pb}/^{204}\text{Pb} \sim 0$ and higher $^{143}\text{Nd}/^{144}\text{Nd}$ ($\epsilon\text{Nd} \sim -8$), which is consistent with Pacific MORB-type
55
56 575 crust in the subduction flux (Fig. 6e). Hahajima is also characterised by a much subdued
57
58 576 enrichment in fluid-mobile elements (lowest Ba/Nb, highest Ce/Pb among volcanics from the
59
60 577 Bonin Islands: Fig. 5a,b). Given the higher Ce/Pb of Hahajima (5-12), it is possible that a
578
579 578 greater proportion of these trace elements were derived from melting of the Indian-MORB-
580
581 579 style mantle wedge (Ce/Pb ~ 25) rather than the subduction fluid (< 2). This is also supported by

1
2
3
4
5
6 580 its higher $\Delta^{208}\text{Pb}/^{204}\text{Pb}$ (~12) and ϵHf (16), which are transitional between the characteristics of
7 581 the Indian mantle domain and a subduction input dominated by Pacific MORB (Fig. 6b, f).
8
9 582

10 583 Slab derived material can take different physical forms, such as supercritical fluid, siliceous
11 584 melt or hydrous fluid. The physical properties are chiefly controlled by temperature (e.g.,
12 585 Kawamoto et al., 2012) as well as pressure and source mineral assemblage. Slab-derived
13 586 material affecting the Quaternary Izu-Bonin frontal arc volcanoes appears to be dominated by
14 587 hydrous fluid; except its southernmost part around Ioto Island (e.g., Taylor and Nesbitt, 1998;
15 588 Ishizuka et al., 2007). Hence, a major difference between the earliest Eocene arc and the modern
16 589 Izu-Bonin arc appears to be that a siliceous melt component was prominent and dominant in
17 590 early arc relative to the modern arc, whatever the nature of the subducting materials. This might
18 591 indicate that in the earliest subarc mantle was hotter at a shallower depth relative to the modern
19 592 arc. Consequently, this allowed the generation of more siliceous melt directly from slab or from
20 593 reactions between supercritical fluids and the mantle, which released melts with a high-Mg
21 594 andesitic composition (e.g., Kessel et al., 2005; Mibe et al., 2011; Kawamoto et al., 2012).
22
23
24
25
26
27
28
29
30
31 595

32 596 **Nature of the subducting slab**

33
34 597
35 598 Bonin Islands magmatism describes the evolution of a nascent arc and indicates that there were
36 599 a series of distinct changes in the subduction flux within a period of 4 million years (Fig. 9a-c).
37 600 Following the Indian MORB-like forearc basalts, the initial high-Si boninite arc magmas at ~48
38 601 Ma reflect a flux of melt or supercritical fluid derived from subducted crust comprising
39 602 accumulations of pelagic sediment on Pacific MORB (Fig. 9a, d).
40
41
42
43

44 603 Following this at 45 Ma, the slab flux briefly switched to originating from a combination of
45 604 HIMU-style sediment and Pacific MORB, before Pacific-MORB became the dominant
46 605 subduction input to the mantle wedge at ~44 Ma. A transient HIMU signature such as this is
47 606 compatible with a 30 km diameter seamount subducted at 4 cm/year, which would take < 1 Myr
48 607 to pass beneath the arc (Fig. 9b, d). This estimate is consistent with the short duration of
49 608 Mikazukiyama group activity with a strong signature of ocean island volcano-derived material.
50 609 After the seamount passed, it appears that the Pacific plate provided a negligible amount of
51 610 sediment, because the Hahajima group are dominated by a signature of Pacific ocean crust (Fig.
52 611 9c, d). This lack of pelagic sediment after 45 Ma might be explained by the following scenarios:
53
54
55
56 612 1) pelagic sediment was absent from areas of the subducting plate e.g. on young ocean crust or
57
58
59
60

1
2
3
4
5
6 613 in an environment not suitable for pelagic sedimentation. 2) Pelagic sediment was not
7 614 subducted because it was scraped off and accreted to the trench slope. 3) Subducting pelagic
8 615 sediment released its melt or fluid flux before it reached the melt generation depth for Hahajima.

9
10 616 Assuming that the Pacific plate was being subducted, a drastic change in the age of the crust
11 617 seems unlikely, except in the presence of hotspot-related seamounts. Variation of the CCD
12 618 could cause a variation in sediment thickness and composition via the abundance of biogenic
13 619 carbonate. Sedimentary carbonate could cause a dilution of all trace elements except Sr (and Sr
14 620 is not highly enriched in currently subducting Izu-Bonin carbonate sediment; Plank et al., 2007).
15 621 This implies that carbonate variation in the subducting sediment probably does not significantly
16 622 change the isotopic composition (at least for Nd and Pb) of subducting sediment. Siliceous
17 623 biogenic sediment can also dilute the enrichment of continentally-derived pelagic clays and/or
18 624 sediments, hence should not affect the isotopic and trace element signature of subducting
19 625 sediment.

20
21 626 Based on recent plate reconstruction models, the location of subduction nucleation for the Izu-
22 627 Bonin arc is predicted to have been far from continents (Seton et al., 2015; Wu et al., 2016).
23 628 Eurasia is the most likely source of terrigenous sediment, but its contribution is expected to
24 629 have been relatively small, and has not changed significantly in this time period. Accordingly,
25 630 it is hard to explain the lack of a sediment signature simply via compositional variation of the
26 631 subducting sediment: an absence of pelagic sediment seems more likely.

27 632 An extensional stress regime on the overriding plate (i.e., the Philippine Sea plate) generated
28 633 spreading and FAB magmatism during the initial stages of subduction. This extension appears
29 634 to have prevailed until the end of boninite magmatism at around 45 Ma (Umino, 1985; Umino
30 635 & Nakano, 2007). After 45 Ma, there is little evidence for the development of a parallel dyke
31 636 swarm. This implies a change in regional stress regime, i.e., a decreasing differential stress
32 637 between σ_1 and σ_3 in the horizontal plane, indicating a cessation of regional extension. This
33 638 change in the stress regime might have been linked to trench retreat and/or a variation in the
34 639 rate of convergence. In turn, these could potentially affect the rate of erosion or accretion at the
35 640 trench (e.g., Clift & Vannucchi, 2004) and hence align with the second scenario above. Lower
36 641 crust and upper mantle are exposed along the Izu-Ogasawara Trench (Ishizuka et al., 2011;
37 642 Morishita et al., 2011), which implies that erosion or extension in the forearc has uncovered the
38 643 deepest arc. The timing of this exposure is not clear, but this implies that the Izu-Ogasawara
39 644 trench was erosional at some point after boninite magmatism, and the accreted sediment, if any,
40 645 could have been removed at any time between the Eocene and present.

1
2
3
4
5
6 646 In terms of the third scenario, some evidence for dehydration of the slab in the forearc can be
7 647 taken from the occurrence of serpentinite derived from mantle harzburgite found in the Izu
8 648 forearc at ODP Sites 783 and 784 (Fryer et al., 1990; Ishii et al., 1992). Kamimura et al. (2002)
9 649 obtained a seismic velocity structure of the Izu forearc including the serpentinite-based
10 650 Torishima Seamount. They proposed that the low velocity in the forearc mantle corresponded
11 651 to serpentinised peridotite hydrated by dehydration of the subducting slab. Serpentinisation of
12 652 the forearc mantle is expected to occur below 600°C, and hence be amagmatic (e.g., Hyndman
13 653 and Peacock, 2003; Ribeiro et al., 2019). Accordingly, even though the age of the
14 654 serpentinisation is not clear, sediment dehydration in the forearc without magmatism is a
15 655 possibility after 45 Ma.

16 656
17 657 The locus of magmatism appears to have migrated by about 80 km within 5 million years from
18 658 near the trench to the Bonin Islands. This does not simply mean that a specific point of the
19 659 subducting slab moved this distance away from the trench as slab flux clearly changed with
20 660 time. However, if we assume a subduction angle of 45° and a minimum subduction rate of
21 661 around 3-4 cm/year, this could explain the migration of volcanic activity. The slab depth is
22 662 expected to be greater than 40 km, based on the depth estimate for melt extraction of boninites
23 663 at 48 Ma (by assuming that melt extraction occurred in the mantle wedge: Umino *et al.*, 2015),
24 664 which is consistent with the above estimate for the rate of subduction.

25 665 Since the locus of Eocene magmatism migrated away from the trench, the chemical
26 666 composition of magmatism is likely to have been influenced by a progressively deeper release
27 667 from the slab. At this time the mantle also was free of earlier metasomatism, i.e. the subduction
28 668 flux was added to a “clean sheet” mantle source. Combining the progressive deepening and the
29 669 initially flux-free mantle may explain why the nascent arc records sharp changes in the slab
30 670 flux compared to the modern mature arc.

31 671

32 672 CONCLUSION

33 673

34 674 High-precision isotope data combined with $^{40}\text{Ar}/^{39}\text{Ar}$ dating constrain the chemical evolution
35 675 of the Izu-Bonin system as it responded to the initiation of subduction. Volcanic activity
36 676 migrated 80 km away from the trench over a period of 5 million years, in response to the
37 677 progressive descent of the slab until the establishment of steady-state subduction.

38 678 1) Following initial spreading and MORB-like magmatism (50-52 Ma), and short period of
39
40
41
42
43
44
45
46
47
48
49
50
51
52
53
54
55
56
57
58
59
60

1
2
3
4
5
6 679 activity of low-Si boninite near axis at 51 Ma, the nascent arc erupted high-Si boninite
7 680 adjacent to the trench (46-50 Ma). This progressed into low-Si boninite and cpx-opx
8 681 andesites (45 Ma), then tholeiitic and calcalkaline magmatism (38.4-45 Ma).

9
10 682 2) These changes in magma type coincided with sharp changes in the slab-derived flux. On
11 683 the Bonin Islands, initial high-Si boninites reflect a pelagic sediment and MORB-derived
12 684 flux. This was replaced by a HIMU-type volcanoclastic signature in the following low-Si
13 685 boninites. In turn, this signature was replaced by a Pacific MORB-dominated flux in the
14 686 post 45 Ma volcanics.

15
16 687 3) Trace element data suggest that the flux-free mantle wedge composition was initially a
17 688 harzburgitic, potentially residual following forearc basalt removal. At 45 Ma this changed
18 689 to a less depleted mantle with characteristics similar to Philippine Sea MORB source.

19 690 4) Changes in slab-flux and mantle wedge composition may be a response to the unique and
20 691 transient conditions following subduction initiation. Subduction-free mantle in the nascent
21 692 arc allowed preservation of a clear time-record of the changing subducted material. In
22 693 maturity, the arc tapped an upwelling asthenosphere that was imparted with an integrated
23 694 average flux reflecting a combination of the sedimentary and ocean crust components.

24 695

25 696 **ACKNOWLEDGEMENTS**

26 697
27 698 We would like to thank K. Yamanobe for preparation of glass beads and assistance with the
28 699 ICP-MS measurements. We appreciate A. Owada, T. Sato and E. Hirabayashi for preparation
29 700 of thin sections. We also thank T. Sasaki, T. Shimono, A. Tokumoto, and H. Nagato for helping
30 701 preparation of rock powder, and N. Geshi and Y. Ishizuka for the maintenance of GSJ XRF
31 702 laboratory. Andy Milton and Agnes Michalik are thanked for assistance in the Southampton
32 703 isotope laboratories. We appreciate IMR, Tohoku University and Oregon State University for
33 704 neutron irradiation. This work was supported by Grant-in-Aid (B) (No. 25287133), (C) (No.
34 705 17K05686) and JSPS bilateral grant (Japan-UK) for OI. The authors acknowledge the
35 706 constructive reviews by anonymous reviewers and helpful editorial comments by Georg
36 707 Zellmer and Marjorie Wilson.

37 708

38 709 **SUPPLEMENTARY DATA**

39 710 Supplementary data are available at Journal of Petrology online.

40 711

41 712 **REFERENCES**

42 60

- 1
2
3
4
5 713
6
7 714 Blichert-Toft, J. & Albarede, F. (1997). The Lu-Hf isotope geochemistry of chondrites and the
8
9 715 evolution of the mantle-crust system. *Earth and Planetary Science Letters* **148**, 243–258.
10
11 716 Chauvel, C., Marini, J.-C., Plank, T. & Ludden, J. (2009). Hf-Nd input flux in the Izu-Mariana
12
13 717 subduction zone and recycling of subducted material in the mantle. *Geochemistry
14 718 Geophysics Geosystems* **10**, 2008GC002101.
15
16 719 Chu, N. C., Taylor, R. N., Chavagnac, V., Nesbitt, R. W., Boella, R. M., Milton, J. A., German,
17
18 720 C. R., Bayon, C. & Burton, K. (2002). Hf isotope ratio analysis using multi-collector
19
20 721 inductively coupled plasma mass spectrometry: an evaluation of isobaric interference
21
22 722 corrections. *Journal of Analytical Atomic Spectrometry* **17**, 1567–1574.
23
24 723 Clift, P. & Vannucchi, P. (2004). Controls on tectonic accretion versus erosion in subduction
25
26 724 zones: Implications for the origin and recycling of the continental crust. *Reviews of
27 725 Geophysics* **42**, RG2001, doi:10.1029/2003RG000127.
28
29 726 Cosca, M. A., Arculus, R. J., Pearce, J. A. & Mitchell, J.G. (1998). $^{40}\text{Ar}/^{39}\text{Ar}$ and K-Ar
30
31 727 geochronological age constraints for the inception and early evolution of the Izu-Bonin-
32
33 728 Mariana arc system. *The Island Arc* **7**, 579-595.
34
35 729 Davidson, J. P., Turner, S., Handley, H., Macpherson, C. & Dosseto, A. (2007). An amphibole
36
37 730 ‘sponge’ in arc crust? *Geology* **35**, 787-790.
38
39 731 Durkin, K., Castillo, P. R., Straub, S. M., Abe, N., Tamura, Y. & Yan, Q. (in press). An origin
40
41 732 of the along-arc compositional variation in the Izu-Bonin arc system. *Geoscience Frontiers*
42
43 733 doi.org/10.1016/j.gsf.2019.12.004.
44
45 734 Fitton, J. G., Saunders, A. D., Norry, M. J., Hardarson, B. S. & Taylor, R.N. (1997). Thermal
46
47 735 and chemical structure of the Iceland plume. *Earth and Planetary Science Letters* **153**, 197–
48
49 736 208.
50
51 737 Fleck, R.J., Sutter, J.F. & Elliot, D.H. (1977). Interpretation of discordant $^{40}\text{Ar}/^{39}\text{Ar}$ age-spectra
52
53 738 of Mesozoic tholeiites from Antarctica. *Geochimica et Cosmochimica Acta* **41**, 15-32.
54
55 739 Fryer, P., Pearce, J. A., Stokking, L. B., et al. (1990). *Proceedings of the Ocean Drilling
56
57 740 Program Initial Reports: Ocean Drilling Program, College Station, TX*, **125**.
58
59 741 Gale A., Dalton, C. A., Langmuir, C. H., Su, Y. & Schilling, J.-G. (2013). The mean
60
742 composition of ocean ridge basalts. *Geochemistry Geophysics Geosystems* **14**,
743 doi:10.1029/2012GC004334.
744 Hall, C.E., Gurnis, M., Sdrolias, M., Lavier, L.L. & Muellar, R.D. (2003). Catastrophic
745 initiation of subduction following forced convergence across fracture zones. *Earth and*

- 1
2
3
4
5
6 746 *Planetary Science Letters* **212**, 15-30.
- 7 747 Hart, S. R. (1984). A large-scale isotopic anomaly in the Southern hemisphere mantle. *Nature*
8 748 **309**, 753–757.
- 9
10 749 Hauff, F., Hoernle, K. & Schmidt, A. (2003). Sr–Nd–Pb composition of Mesozoic Pacific
11 750 oceanic crust (Site 1149 and 801, ODP Leg 185): implications for alteration of ocean crust
12 751 and the input into the Izu-Bonin-Mariana subduction system. *Geochemistry Geophysics*
13 752 *Geosystems* **4(8)**,8913, doi:10.1029/2002GC000421.
- 14 753 Hickey-Vargas, R. (1991). Isotope characteristics of submarine lavas from the Philippine Sea:
15 754 implications for the origin of arc and basin magmas of the Philippine tectonic plate. *Earth*
16 755 *and Planetary Science Letters* **107**, 290-304.
- 17 756 Hickey-Vargas, R., Hergt, J. M. & Spadea, P. (1995). The Indian Ocean-type isotopic signature
18 757 in Western Pacific marginal basins. In: Taylor B. & Natland, J. (eds) *Origin and significance*
19 758 *in Active Margins and Marginal Basins of the Western Pacific*. American Geophysical Union,
20 759 *Geophysical Monograph* **88**, 175-197.
- 21 760 Hickey-Vargas, R. (1998). Origin of the Indian Ocean-type isotopic signature in basalts from
22 761 Philippine Sea Plate spreading centers: An assessment of local versus large-scale processes.
23 762 *Journal of Geophysical Research* **103**, 20963-20979.
- 24 763 Hickey-Vargas, R., Yogodzinski, G. M., Ishizuka, O., McCarthy, A., Bizimis, M., Kusano, Y.,
25 764 Savov, I. P. & Arculus, R. (2018). Origin of depleted basalts during subduction initiation and
26 765 early development of the Izu-Bonin-Mariana Island arc: Evidence from IODP Expedition
27 766 351 Site U1438, Amami-Sankaku Basin. *Geochimica et Cosmochimica Acta* **229**, 85–111.
- 28 767 Hyndman, R. D. & Peacock, S. M. (2003). Serpentinization of the forearc mantle. *Earth and*
29 768 *Planetary Science Letters* **212**, 417-432.
- 30 769 Ishii, T., Robinson, P. T., Maekawa, H. & Fiske, R. (1992). Petrological studies of peridotites
31 770 from diapiric serpentinite seamounts in the Izu-Ogasawara–Mariana forearc, Leg 125.
32 771 *Proceedings of the Ocean Drilling Program Scientific Results* **125**, 445–485.
- 33 772 Ishizuka, O., Taylor, R. N., Milton, J. A. & Nesbitt, R. W. (2003). Fluid-mantle interaction in
34 773 an intra-oceanic arc: constraints from high-precision Pb isotopes. *Earth and Planetary*
35 774 *Science Letters* **211**, 221-236.
- 36 775 Ishizuka, O., Kimura, J., Li, Y., Stern, R., Reagan, M., Taylor, R., Ohara, Y., Bloomer, S., Ishii,
37 776 T. & Hargrove III, U. (2006a). Early stages in the evolution of Izu–Bonin arc volcanism:
38 777 new age, chemical, and isotopic constraints. *Earth and Planetary Science Letters* **250**, 385-
39 778 401.
- 40
41
42
43
44
45
46
47
48
49
50
51
52
53
54
55
56
57
58
59
60

- 1
2
3
4
5
6 779 Ishizuka, O., Taylor, R. N., Milton J. A., Nesbitt, R. W., Yuasa, M. & Sakamoto, I. (2006b).
7 780 Variation in the source mantle of the northern Izu arc with time and space -Constraints from
8 781 high-precision Pb isotopes -. *Journal of Volcanology and Geothermal Research* **156**, 266-
9 782 290.
- 12 783 Ishizuka, O., Taylor, R. N., Milton J. A., Nesbitt, R. W., Yuasa, M. & Sakamoto, I. (2007).
14 784 Processes controlling along-arc isotopic variation of the southern Izu-Bonin arc.
15 785 *Geochemistry Geophysics Geosystems* **8**, Q06008, doi:10.1029/2006GC001475.
- 17 786 Ishizuka, O., Yuasa, M., Taylor, R. N. & Sakamoto, I. (2009). Two contrasting magmatic types
18 787 coexist after the cessation of back-arc spreading. *Chemical Geology* **266**, 283-305.
- 21 788 Ishizuka, O., Yuasa, M., Tamura, Y., Shukuno, H., Stern, R. J., Naka, J., Joshima, M. & Taylor,
22 789 R. N. (2010). Migrating shoshonitic magmatism tracks Izu-Bonin-Mariana intra-oceanic arc
23 790 rift propagation. *Earth and Planetary Science Letters* **294**, 111-122.
- 26 791 Ishizuka, O., Tani, K., Reagan, M. K., Kanayama, K., Umino, S., Harigane, Y., Sakamoto, I.,
27 792 Miyajima, Y., Yuasa, M. & Dunkley, D.J. (2011a). The timescales of subduction initiation
28 793 and subsequent evolution of an oceanic island arc. *Earth and Planetary Science Letters* **306**,
29 794 229-240.
- 32 795 Ishizuka, O., Taylor, R. N., Yuasa, M. & Ohara, Y. (2011b). Making and breaking an Island
33 796 arc: a new perspective from the Oligocene Kyushu-Palau arc, Philippine Sea. *Geochemistry*
34 797 *Geophysics Geosystems* **12**, Q05005, doi:10.1029/2010GC003440.
- 37 798 Ishizuka, O., Taylor, R. N., Ohara, Y. & Yuasa, M. (2013). Upwelling, rifting and age-
38 799 progressive magmatism from the Oki-Daito mantle plume. *Geology* **41**, 1011-1014.
- 41 800 Ishizuka, O., Tani, K. & Reagan, M. K. (2014a). Izu-Bonin-Mariana fore-arc crust as a modern
42 801 ophiolite analogue. *Elements* **10**, 115-120.
- 44 802 Ishizuka, O., Umino, S., Taylor, R. N. & Kanayama, K. (2014b). Evidence for hydrothermal
45 803 activity in the earliest stages of intraoceanic arc formation: implication to ophiolite-hosted
46 804 hydrothermal activity. *Economic Geology* **109**, 2159-2177.
- 49 805 Ishizuka, O., Hickey-Vargas, R., Arculus, R. J., Yogodzinski, G. M., Savov, I. P., Kusano, Y.,
50 806 McCarthy, A., Brandl, P. & Sudo, M. (2018). Age of Izu-Bonin-Mariana arc basement. *Earth*
51 807 *and Planetary Science Letters* **481**, 80-90.
- 54 808 Johnson, C. M. & Beard, B. L. (1999). Correction of instrumentally produced mass
55 809 fractionation during isotopic analysis of Fe by thermal ionization mass spectrometry.
56 810 *International Journal of Mass Spectrometry* **193**, 87-99.
- 59 811 Kamimura, A., Kasahara, J., Shinohara, M., Hino, R., Shiobara, H., Fujie, G. & Kanazawa, T.
60

- 1
2
3
4
5
6 812 (2002). Crustal structure study at the Izu-Bonin subduction zone around 31°N: implications
7 813 of serpentinized materials along the subduction plate boundary. *Physics of the Earth and*
8 814 *Planetary Interiors* **132**, 105–129, doi:10.1016/S0031-9201(02)00047-X.
- 9
10 815 Kanayama, K., Umino, S. & Ishizuka, O. (2012). Eocene volcanism during the incipient stage
11 816 of Izu–Ogasawara Arc: Geology and petrology of the Mukojima Island Group, the
12 817 Ogasawara Islands. *The Island Arc* **21**, 288–316.
- 13
14 818 Kanayama, K., Umino, S. & Ishizuka, O. (2014). Shallow submarine volcano group in the early
15 819 stage of island arc development: Geology and petrology of small islands south off Hahajima
16 820 main island, the Ogasawara Islands. *Journal of Asian Earth Sciences* **85**, 1–25.
- 17
18 821 Kawamoto, T., Kanzaki, M., Mibe, K., Matsukage, K. N. & Ono, S. (2012). Separation of
19 822 supercritical slab-fluids to form aqueous fluid and melt components in subduction zone
20 823 magmatism. *Proceedings of the National Academy of Sciences of the United States of*
21 824 *America* **109**, 18695–18700.
- 22
23 825 Kelley, K. A., Plank, T., Ludden, J. & Staudigel, H. (2003). Composition of altered oceanic
24 826 crust at ODP Sites 801 and 1149. *Geochemistry Geophysics Geosystems* **4**(6),
25 827 doi:10.1029/2002GC000435.
- 26
27 828 Kessel, R., Schmidt, M. W., Ulmer, P. & Pettke, T. (2005). Trace element signature of
28 829 subduction-zone fluids, melts and supercritical liquids at 120–180km depth. *Nature* **437**(29),
29 830 724–727.
- 30
31 831 Koppers, A. A. P., Staudigel, H., Wijbrans, J. R. & Pringle, M. S. (1998). The Magellan
32 832 seamount trail: implications for Cretaceous hotspot volcanism and absolute Pacific plate
33 833 motion. *Earth and Planetary Science Letters* **163**, 53–68.
- 34
35 834 Koppers, A. A. P., Staudigel, H., Pringle, M. S. & Wijbrans, J. R. (2003). Short-lived and
36 835 discontinuous intraplate volcanism in the South Pacific: Hot spots or extensional volcanism?
37 836 *Geochemistry Geophysics Geosystems* **4**(10), doi:10.1029/2003GC000533.
- 38
39 837 Li, H. -Y., Taylor, R. N., Prytulak, J., Kirchenbaur, M., Shervais, J. W., Ryan, J. G., Godard,
40 838 M., Reagan, M. & Pearce, J. A. (2019). Radiogenic isotopes document the start of subduction
41 839 in the Western Pacific. *Earth and Planetary Science Letters* **518**, 197–210.
- 42
43 840 Li, Y. -B., Kimura, J. -I., Machida, S., Ishii, T., Ishiwatari, S., Maruyama, S., Qiu, N.-N.,
44 841 Ishikawa, T., Kato, Y., Haraguchi, S., Takahata, N., Hirahara, Y. & Miyazaki, T. (2013).
45 842 High-Mg adakite and low-Ca boninite from a Bonin fore-arc seamount: implications for the
46 843 reaction between slab melts and depleted mantle. *Journal of Petrology* **54**, 1149–1175.
- 47
48 844 Mibe, K., Kawamoto, T., Matsukage, K. N., Fei, Y. & Ono, S. (2011) Slab melting versus slab
49
50
51
52
53
54
55
56
57
58
59
60

- 1
2
3
4
5
6 845 dehydration in subduction-zone magmatism. *Proceedings of the National Academy of*
7 846 *Sciences of the United States of America* **1088**, 177–8182.
- 9 847 Miyashiro, A. (1974). Volcanic rock series in island arcs and active continental margins.
10 848 *American Journal of Science* **257**, 609-647.
- 12 849 Miyazaki, T., Kimura, J.-I., Senda, R., Bogdan, V., Chang, Q., Takahashi, T., Hirahara, Y.,
14 850 Hauff, F., Hayasaka, Y., Sano, S., Shimoda, G., Ishizuka, O., Kawabata, H., Hirano, N.,
16 851 Machida, S., Ishii, T., Tani, K. & Yoshida, T. (2015). Missing western half of the Pacific
17 852 Plate: Geochemical nature of the Izanagi-Pacific Ridge interaction with a stationary
19 853 boundary between the Indian and Pacific mantles. *Geochemistry, Geophysics, Geosystems*
21 854 **16**, 3309-3332.
- 23 855 Plank, T. & Langmuir, C. H. (1998). The chemical composition of subducting sediment and its
24 856 consequences for the crust and mantle. *Chemical Geology* **145**, 325-394.
- 26 857 Plank, T., Kelley, K. A., Murray, R. W. & Stern, L. Q. (2007). Chemical composition of
27 858 sediments subducting at the Izu-Bonin trench. *Geochemistry, Geophysics, Geosystems* **8**,
29 859 Q04I16, doi:10.1029/2006GC001444.
- 31 860 Reagan, M. K., Ishizuka, O., Stern, R. J., Kelley, K. A., Ohara, Y., Blichert-Toft J., Bloomer,
32 861 S. H., Cash, J., Fryer, P., Hanan, B. B., Hickey-Vargas, R., Ishii, T., Kimura, J. I., Peate, D.
34 862 W., Rowe, M. C. & Woods, M. (2010). Fore-arc basalts and subduction initiation in the Izu-
35 863 Bonin-Mariana system. *Geochemistry, Geophysics, Geosystems* **11**, Q03X12,
37 864 doi:10.1029/2009GC002871.
- 39 865 Reagan, M. K., Pearce, J. A., Petronotis, K., Almeev, R. R., Avery, A. J., Carvallo, C., Chap-
41 866 man, T., Christeson, G. L., Ferré, E. C., Godard, M., Heaton, D. E., Kirchenbaur, M., Kurz,
43 867 W., Kutterolf, S., Li, H., Michibayashi, K., Morgan, S., Nelson, W. R., Prytulak, J., Python,
44 868 M., Robertson, A. H. F., Ryan, J. G., Sager, W. W., Sakuyama, T., Shervais, J. W., Shimizu,
46 869 K. & Whattam, S.A. (2017). Subduction initiation and ophiolite crust: new insights from
47 870 IODP drilling. *International Geology Review* **59**, DOI: 10.1080/00206814.2016.1276482.
- 49 871 Reagan, M. K., Heaton, D. E., Schmitz, M. D., Pearce, J. A., Shervais, J. W. & Koppers, A. A.
51 872 P. (2019). Forearc ages reveal extensive shortlived and rapid seafloor spreading following
52 873 subduction initiation. *Earth and Planetary Science Letters* **506**, 520–529.
- 54 874 Ribeiro, J., Ishizuka, O., Lee, C-T. A. & Girard, G. (2019). Evolution and maturation of the
55 875 nascent Mariana arc. *Earth and Planetary Science Letters* **530**,
57 876 <https://doi.org/10.1016/j.epsl.2019.115912>.
- 59 877 Savov, I. P., Hickey-Vargas, R., D'Antonio, M., Ryan, J. G. & Spadea, P. (2006). Petrology
60

- 1
2
3
4
5
6 878 and geochemistry of West Philippine Basin basalts and early Palau-Kyushu arc volcanic
7 879 clasts from ODP Leg 195, Site 1201D: Implications for the early history of the Izu-Bonin-
8 880 Mariana Arc. *Journal of Petrology* **47**, 277-299.
- 9
10 881 Seton, M., Flament, N., Whittaker, J., Müller, R. D., Gurnis, M. & Bower, D. J. (2015). Ridge
11 882 subduction sparked reorganization of the Pacific plate-mantle system 60–50 million years
12 883 ago. *Geophysical Research Letters* **42**, 1732–1740.
- 13
14 884 Shervais, J. W., Reagan, M., Haugen, E., Almeev, R. R., Pearce, J. A., Prytulak, J., Ryan, J. G.,
15 885 Whattam, S. A., Godard, M., Chapman, T., Li, H., Kurz, W., Nelson, W., Heaton, D.,
16 886 Kirchenbaur, M., Shimizu, K., Sakuyama, T., Li, Y. & Vetter, S. K. (2019). Magmatic
17 887 response to subduction initiation: Part 1. Fore-arc basalts of the Izu-Bonin arc from IODP
18 888 Expedition 352. *Geochemistry, Geophysics, Geosystems* **20**,
19 889 <https://doi.org/10.1029/2018GC007731>.
- 20
21 890 Steiger, R. H. & Jäger, E. (1977). Subcommittee on Geochronology: convention on the use of
22 891 decay constants in geo- and cosmochemistry. *Earth and Planetary Science Letters* **36**, 359-
23 892 362.
- 24
25 893 Stern, R. J. & Bloomer, S. H. (1992). Subduction zone infancy: examples from the Eocene Izu-
26 894 Bonin-Mariana and Jurassic California Arcs. *Geological Society of America Bulletin* **104**,
27 895 1621-1636.
- 28
29 896 Stern, R. J. (2004). Subduction Initiation: Spontaneous and Induced. *Earth and Planetary*
30 897 *Science Letters* **226**, 275-292.
- 31
32 898 Stern, R. J., Reagan, M., Ishizuka, O., Ohara, Y. & Whattam, S. (2012). To understand
33 899 subduction initiation, study forearc crust; to understand forearc crust, study ophiolites.
34 900 *Lithosphere* **4**, 469–483.
- 35
36 901 Straub, S. M., Goldstein, S. L., Class, C. & Schmidt, A. (2009). Mid-ocean-ridge basalt of
37 902 Indian type in the northwest Pacific Ocean basin. *Nature Geoscience* **2**, 286-289.
- 38
39 903 Straub, S. M., Woodhead, J. D. & Arculus, R. J. (2015). Temporal evolution of the Mariana
40 904 Arc: mantle wedge and subducted slab controls revealed with a tephra perspective. *Journal*
41 905 *of Petrology* **56**, 409–439.
- 42
43 906 Tanaka, T., Togashi, S., Kamioka, H., Amakawa, H., Kagami, H., Hamamoto, T., Yuhara, M.,
44 907 Orihashi, Y., Yoneda, S., Shimizu, H., Kunimaru, T., Takahashi, K., Yanagi, T., Nakano, T.,
45 908 Fujimaki, H., Shinjo, R., Asahara, Y., Tanimizu, M. & Dragusanu, C. (2000). JNdi-1: a
46 909 neodymium isotopic reference in consistency with LaJolla neodymium. *Chemical Geology*
47 910 **168**, 279-281.

- 1
2
3
4
5
6 911 Taylor, B. (1992). Rifting and the volcanic-tectonic evolution of the Izu-Bonin-Mariana Arc.
7 912 In: Taylor B. & Fujioka K. et al., (eds) *Proceedings of the Ocean Drilling Program, Scientific*
8 913 *Results* **126**, 627-651.
- 9
10 914 Taylor, R. N., Nesbitt, R. W., Vidal, P., Harmon, R. S., Auvray, B. & Croudace, I. W. (1994).
11 915 Mineralogy, chemistry, and genesis of the Boninite Series Volcanics, Chichijima, Bonin
12 916 Islands, Japan. *Journal of Petrology* **35**, 577-617.
- 13
14 917 Taylor, R. N. & Nesbitt, R. W. (1995). Arc volcanism in an extensional regime at the initiation
15 918 of subduction: A geochemical study of Hahajima, Bonin Islands, Japan. In: Smellie, J. (ed)
16 919 *Volcanism associated with Extension at Consuming Plate Margins*. Geological Society,
17 920 London, Special Publications **81**, 115-134.
- 18
19 921 Taylor, R. N. & Nesbitt, R. W. (1998). Isotopic characteristics of subduction fluids in an intra-
20 922 oceanic setting, Izu-Bonin Arc, Japan. *Earth and Planetary Science Letters* **164**, 79-98.
- 21
22 923 Taylor, R. N., Ishizuka, O., Michalik, A., Milton, J. A. & Croudace, I. W. (2015). Evaluating
23 924 the precision of Pb isotope measurement by mass spectrometry. *Journal of Analytical Atomic*
24 925 *Spectrometry* **30**, 198-213.
- 25
26 926 Thirlwall, M. E. (1991). Long-term reproducibility of multicollector Sr and Nd isotope ratio
27 927 analysis. *Chemical Geology (Isotope Geoscience Section)* **94**, 85-104.
- 28
29 928 Uchiumi, S. & Shibata, K. (1980). Errors in K-Ar age determination. *Bulletin of Geological*
30 929 *Survey of Japan* **31**, 267-273 (in Japanese with English abstract).
- 31
32 930 Umino, S. (1985). Volcanic geology of Chichijima, the Bonin Islands (Ogasawara Islands). *The*
33 931 *Journal of the Geological Society of Japan* **91**, 505-523.
- 34
35 932 Umino, S. & Nakano, S. (2007). *Geology of the Chichijima Retto District*. Quadrangle Series,
36 933 1:50000, Geological Survey of Japan, AIST, 63p (in Japanese with English abstract).
- 37
38 934 Umino, S., Nakano, S., Ishizuka, O. & Komazawa, M. (2009). *Geological Map of Japan*
39 935 *1:200,000, Ogasawara Shoto* (in Japanese). Geological Survey of Japan, AIST.
- 40
41 936 Umino, S., Kitamura, K., Kanayama, K., Tamura, A., Sakamoto, N., Ishizuka, O. & Arai, S.
42 937 (2015). Thermal and chemical evolution of the subarc mantle revealed by spinel-hosted melt
43 938 inclusions in boninite from the Ogasawara (Bonin) Archipelago. *Geology* **43**, 151-154.
- 44
45 939 Umino, S., Ishizuka, O. & Kanayama, K. (2016). *Geology of the Hahajima Retto district*.
46 940 Quadrangle Series, 1:50000, Geological Survey of Japan, AIST, 46p (in Japanese with
47 941 English abstract).
- 48
49
50
51
52
53
54
55
56
57
58
59
60

- 1
2
3
4
5
6 942 Umino, S., Kanayama, K., Kitamura, K., Tamura, A., Ishizuka, O., Senda, R. & Arai, S. (2018).
7 943 Did boninite originate from the heterogeneous mantle with recycled ancient slab? *Island Arc*
8 944 **27**, e12221, doi: 10.1111/iar.12221.
- 9
10 945 Willbold, M. & Stracke, A. (2006). Trace element composition of mantle end-members:
11 946 Implications for recycling of oceanic and upper and lower continental crust, *Geochemistry*
12 947 *Geophysics Geosystems* **7**, Q04004, doi:10.1029/2005GC001005.
- 13
14 948 Woodhead J., Hergt J., Davidson J. P. & Eggins S. M. (2001). Hafnium isotope evidence
15 949 for 'conservative' element mobility during subduction zone processes. *Earth and Planetary*
16 950 *Science Letters* **192**, 331–346.
- 17
18 951 Wu, J., Suppe, J., Lu, R. & Kanda, R. (2016). Philippine Sea and East Asian plate tectonics
19 952 since 52 Ma constrained by new subducted slab reconstruction methods. *Journal of*
20 953 *Geophysical Research* **121**, 4670–4741.
- 21
22 954 Yogodzinski, G., Bizimis, M., Hickey-Vargas, R., McCarthy, A., Hocking, B. D., Savov, I. P.,
23 955 Ishizuka, O. & Arculus, R. (2018). Implications of Eocene-age Philippine Sea and Forearc
24 956 basalts for initiation and early history of the Izu-Bonin-Mariana arc. *Geochimica et*
25 957 *Cosmochimica Acta* **228**, 136-156.
- 26
27 958 York, D. (1969). Least squares fitting of a straight line with correlated errors. *Earth and*
28 959 *Planetary Science Letters* **5**, 320-324.
- 29
30 960 Zindler, A. & Hart, S. (1986). Chemical geodynamics. *Annual Review of Earth and Planetary*
31 961 *Sciences* **14**, 493-571.
- 32
33
34
35
36
37
38
39
40
41
42
43
44
45
46
47
48
49
50
51
52
53
54
55
56
57
58
59
60

1
2
3
4
5
6 975 **Figure captions**

7 976

8
9 977 Fig. 1. a) Overview of the bathymetry of the Izu-Bonin-Mariana arc and location of the Bonin
10 978 Ridge, b) Location of the Bonin Islands with bathymetric map of the Bonin Ridge. Locations
11 979 of studied islands and submarine sampling stations are shown with the symbols used in the
12 980 geochemical plots. (Ishizuka *et al.*, 2006a, 2011a; Reagan *et al.*, 2017). Fig. 1a and 1b are
13 981 modified from Ishizuka *et al.* (2011a). Distribution of each rock type is indicated by the black
14 982 dashed lines.

15 983 Fig. 2. Schematic stratigraphic section and overall chemostratigraphic variation through the
16 984 Bonin Ridge forearc crust. Rock types and symbols shown in this figure remain consistent
17 985 through the geochemical plots in all figures. Average content of SiO₂, CaO and TiO₂ projected
18 986 to 8% MgO (Si8, Ca8 and Ti8) for each stratigraphic unit are shown in the columns to the right.

19 987 Fig. 3. ⁴⁰Ar/³⁹Ar age spectra and Ca/K plots for groundmass samples from the Bonin Islands.

20 988 Fig. 4. Major element composition of volcanic rocks from the Bonin Islands. Variation of
21 989 SiO₂ with a) MgO, b) FeO*(FeO^{total})/MgO (Line distinguishing the tholeiitic and calc-alkaline
22 990 field is from Miyashiro (1974)), and variation of MgO with c) TiO₂, and d) CaO. Data of
23 991 boninites from IODP Exp. 352 are from Li *et al.* (2019).

24 992 Fig. 5. Incompatible trace element ratios for the Bonin Islands. Variation of a) Ce/Pb, b)
25 993 Ba/Nb, c) Th/Ce, d) La/Sm, e) Dy/Yb with SiO₂ in wt%, f) Sm/Zr with Sm in ppm and g) Nb/Zr
26 994 with MgO in wt%. Data of boninites from IODP Exp. 352 are from Li *et al.* (2019). Symbols
27 995 as in Fig. 4. Average trace element ratios for all normal MORB (Gale *et al.*, 2013) are shown.
28 996 Dashed line with arrow in each plot (where the partition coefficient data is available)
29 997 qualitatively show effect of fractionation of amphibole as a guide based on partition coefficients
30 998 for basalt and andesite compiled in the GERM data base (<https://earthref.org>).

31 999 Fig. 6. Radiogenic isotope variation for the Bonin Islands plotted with potential slab and
32 1000 mantle components. a) $\Delta^{207}\text{Pb}/^{204}\text{Pb}$ vs. $^{206}\text{Pb}/^{204}\text{Pb}$, b) $\Delta^{208}\text{Pb}/^{204}\text{Pb}$ vs. $^{206}\text{Pb}/^{204}\text{Pb}$, c)
33 1001 $\Delta^{207}\text{Pb}/^{204}\text{Pb}$ vs. $^{207}\text{Pb}/^{204}\text{Pb}$, d) ϵNd vs. $^{87}\text{Sr}/^{86}\text{Sr}$, e) ϵNd vs. $^{206}\text{Pb}/^{204}\text{Pb}$, f) ϵHf vs. ϵNd .
34 1002 Assumed compositions of subducting igneous crust and sediment are shown (Table S7). Pelagic
35 1003 sediment outboard of Izu-Bonin arc: Plank *et al.* (2007), Pelagic sediment outboard of Mariana
36 1004 arc: Plank & Langmuir (1998), Subducting altered igneous Pacific crust: Hauff *et al.* (2003),
37 1005 volcanoclastic sediment derived from HIMU oceanic islands: Plank & Langmuir (1998).
38 1006 Philippine Sea MORB: Hickey-Vargas (1991, 1998), Savov *et al.* (2006), Ishizuka *et al.* (2009,
39 1007 2010, 2011b, 2013). Pacific MORB data was compiled from the Earthchem data base

1
2
3
4
5
6 1008 (<https://www.earthchem.org>). Least squares regression lines are shown in Pb isotopic plots for
7 1009 some rock types with sufficient data. Symbols are as on Fig. 4. Isotopic ratios plotted in these
8
9 1010 figures are not age-corrected.

10
11 1011 Fig. 7. Isotope versus trace element ratio plots for the Bonin Islands volcanics. Data sources
12 1012 are the same as for Figure 6. Least squares regression lines are shown in panel b. Symbols as
13
14 1013 in Fig. 4.

15
16 1014 Fig. 8. Nb/Zr vs. $^{206}\text{Pb}/^{204}\text{Pb}$ plot. A vector towards volcanoclastic sediment derived from
17 1015 HIMU oceanic islands is shown (Plank & Langmuir, 1998). Symbols as in Fig. 4.

18
19 1016 Fig. 9. Schematic diagram showing the progressive variation in the nature of the slab flux
20 1017 following subduction initiation. a) Chichijima/Mukojima group, 48-45 Ma: shallow melting
21 1018 (~35 km) with flux from pelagic sediment and Pacific Ocean igneous crust added to a
22
23 1019 harzburgitic mantle; b) Mikazukiyama group, 45-44 Ma: melting at ~35 km, slightly further
24 1020 from the trench, flux from HIMU volcanoclastic sediment added to a less depleted mantle
25
26 1021 source; c) Hahajima group, <45 Ma: deeper melting (~60 km) further from the trench with flux
27 1022 from Pacific Ocean crust added to an upwelling, more fertile mantle source. d) Schematic
28
29 1023 diagram showing the estimated scale and duration of flux components on the subducting slab.
30
31
32
33
34
35
36
37
38
39
40
41
42
43
44
45
46
47
48
49
50
51
52
53
54
55
56
57
58
59
60

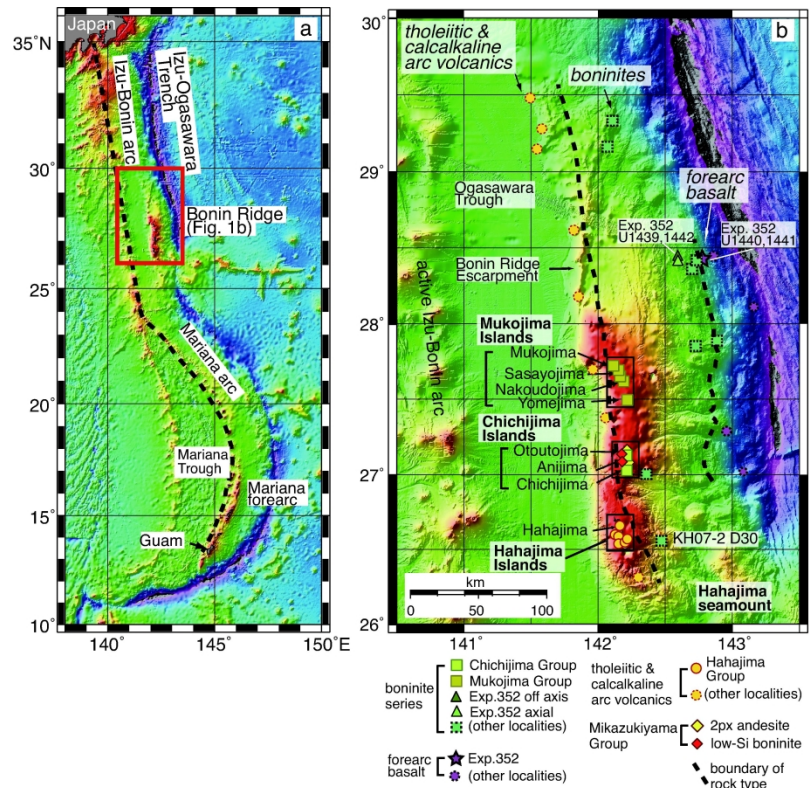


Fig. 1 Ishizuka et al.

Fig. 1. a) Overview of the bathymetry of the Izu-Bonin-Mariana arc and location of the Bonin Ridge, b) Location of the Bonin Islands with bathymetric map of the Bonin Ridge. Locations of studied islands and submarine sampling stations are shown with the symbols used in the geochemical plots. (Ishizuka et al., 2006a, 2011a; Reagan et al., 2017). Fig. 1a and 1b are modified from Ishizuka et al. (2011a). Distribution of each rock type is indicated by the black dashed lines.

146x211mm (600 x 600 DPI)

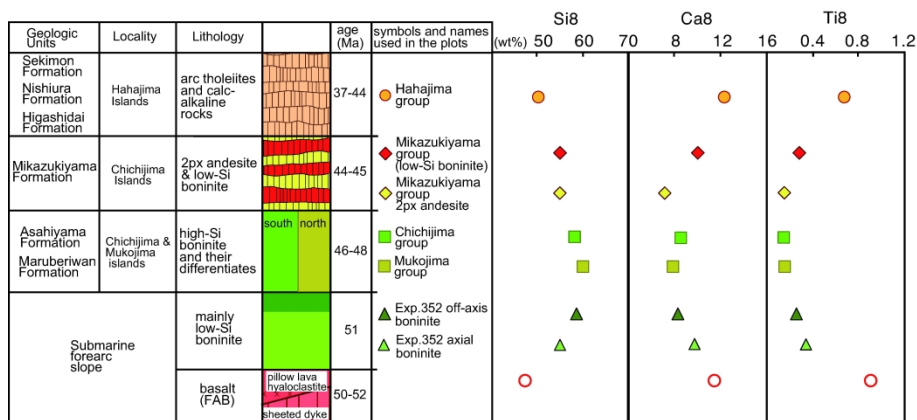


Fig. 2 Ishizuka et al.

Fig. 2. Schematic stratigraphic section and overall chemostratigraphic variation through the Bonin Ridge forearc crust. Rock types and symbols show in this figure remain consistent through the geochemical plots in all figures. Average content of SiO₂, CaO and TiO₂ projected to 8% MgO (Si8, Ca8 and Ti8) for each stratigraphic unit are shown in the columns to the right.

196x252mm (600 x 600 DPI)

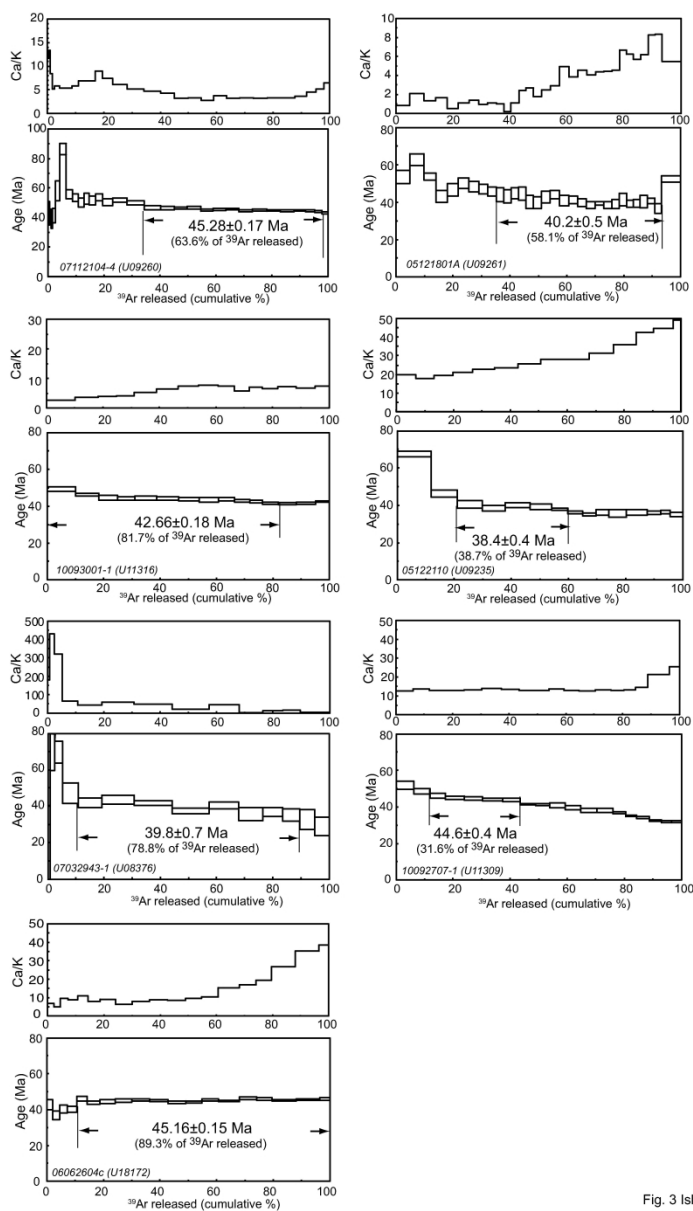


Fig. 3 Ishizuka et al.

Fig. 3. $^{40}\text{Ar}/^{39}\text{Ar}$ age spectra and Ca/K plots for groundmass samples from the Bonin Islands.

177x281mm (600 x 600 DPI)

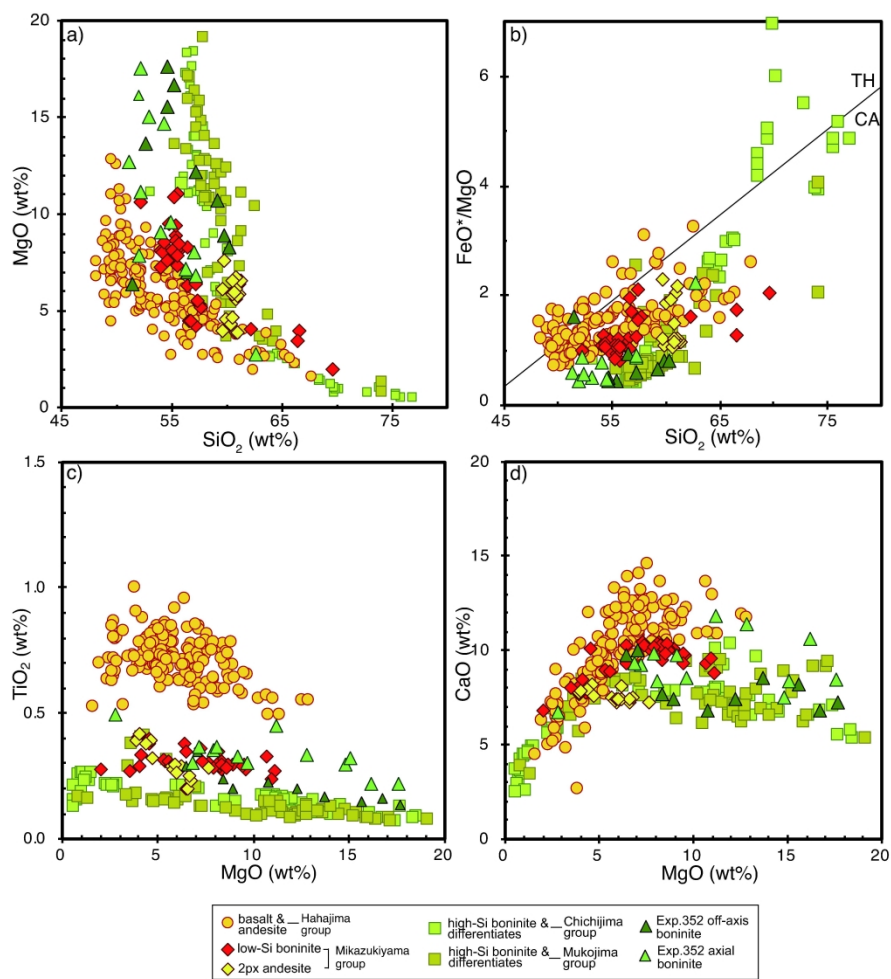


Fig. 4 Ishizuka et al.

Fig. 4. Major element composition of volcanic rocks from the Bonin Islands. Variation of SiO₂ with a) MgO, b) FeO*(FeO_{total})/MgO (Line distinguishing the tholeiitic and calc-alkaline field is from Miyashiro (1974)), and variation of MgO with c) TiO₂, and d) CaO. Data of boninites from IODP Exp. 352 are from Li et al. (2019).

186x253mm (600 x 600 DPI)

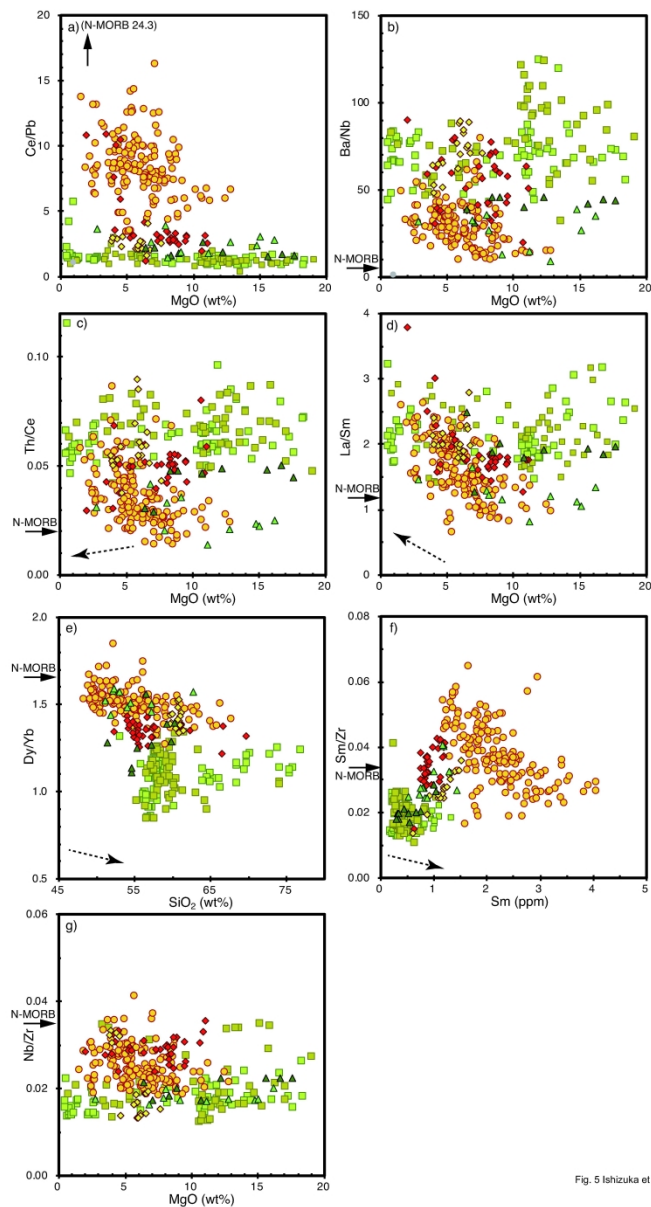


Fig. 5 Ishizuka et al.

Fig. 5 Incompatible trace element ratios for the Bonin Islands. Variation of a) Ce/Pb, b) Ba/Nb, c) Th/Ce, d) La/Sm, e) Dy/Yb with SiO₂ in wt%, f) Sm/Zr with Sm in ppm and g) Nb/Zr with MgO in wt%. Data of boninites from IODP Exp. 352 are from Li et al. (2019). Symbols as in Fig. 4. Average trace element ratios for all normal MORB (Gale et al., 2013) are shown. Dashed line with arrow in each plot (where the partition coefficient data is available) qualitatively show effect of fractionation of amphibole as a guide based on partition coefficients for basalt and andesite compiled in the GERM data base (<https://earthref.org>).

160x289mm (600 x 600 DPI)

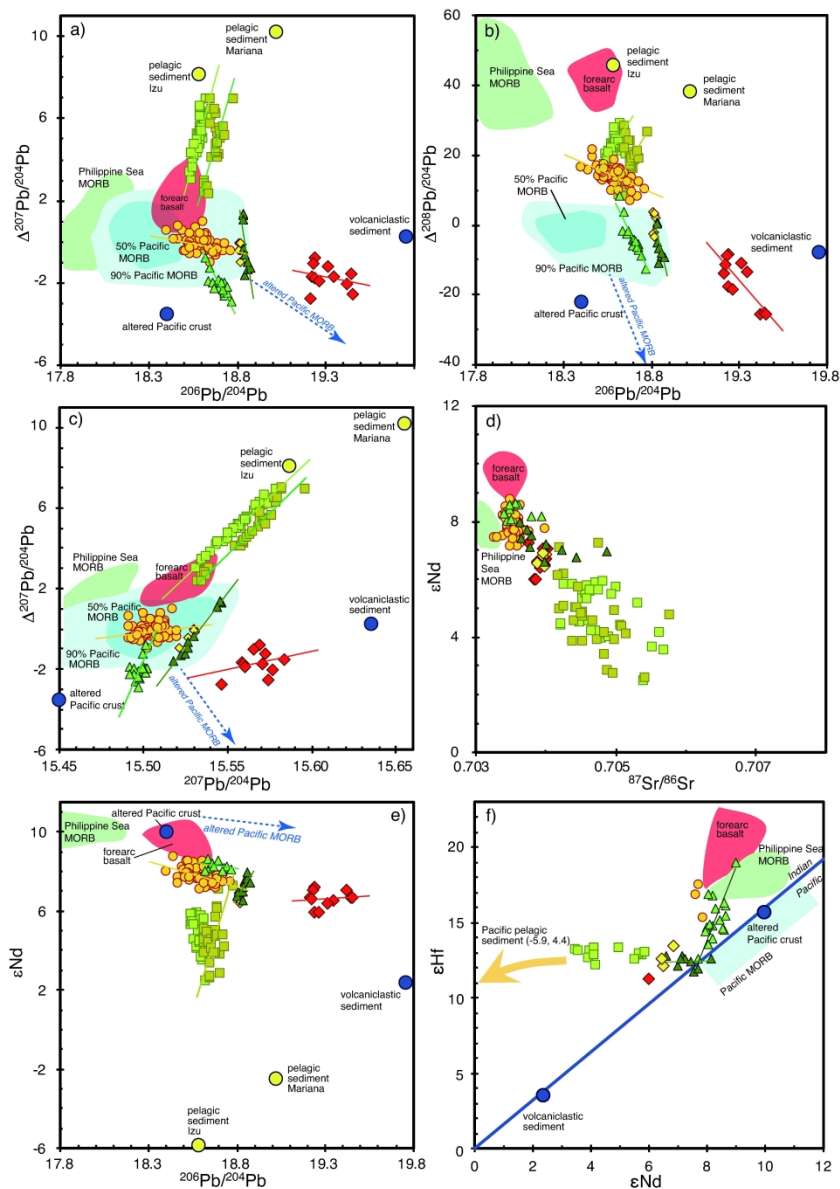


Fig. 6 Ishizuka et al.

Fig. 6. Radiogenic isotope variation for the Bonin Islands plotted with potential slab and mantle components. a) $\Delta^{207}\text{Pb}/^{204}\text{Pb}$ vs. $^{206}\text{Pb}/^{204}\text{Pb}$, b) $\Delta^{208}\text{Pb}/^{204}\text{Pb}$ vs. $^{206}\text{Pb}/^{204}\text{Pb}$, c) $\Delta^{207}\text{Pb}/^{204}\text{Pb}$ vs. $^{207}\text{Pb}/^{204}\text{Pb}$, d) ϵNd vs. $^{87}\text{Sr}/^{86}\text{Sr}$, e) ϵNd vs. $^{206}\text{Pb}/^{204}\text{Pb}$, f) ϵHf vs. ϵNd . Assumed compositions of subducting igneous crust and sediment are shown (Table S7). Pelagic sediment outboard of Izu-Bonin arc: Plank et al. (2007), Pelagic sediment outboard of Mariana arc: Plank & Langmuir (1998), Subducting altered igneous Pacific crust: Hauff et al. (2003), volcanoclastic sediment derived from HIMU oceanic islands: Plank & Langmuir (1998). Philippine Sea MORB: Hickey-Vargas (1991, 1998), Savov et al. (2006), Ishizuka et al. (2009, 2010, 2011b, 2013). Pacific MORB data was compiled from the Earthchem data base (<https://www.earthchem.org>). Least squares regression lines are shown in Pb isotopic plots for some rock types with sufficient data. Symbols are as on Fig. 4. Isotopic ratios plotted in these figures are not age-corrected.

205x289mm (600 x 600 DPI)

1
2
3
4
5
6
7
8
9
10
11
12
13
14
15
16
17
18
19
20
21
22
23
24
25
26
27
28
29
30
31
32
33
34
35
36
37
38
39
40
41
42
43
44
45
46
47
48
49
50
51
52
53
54
55
56
57
58
59
60

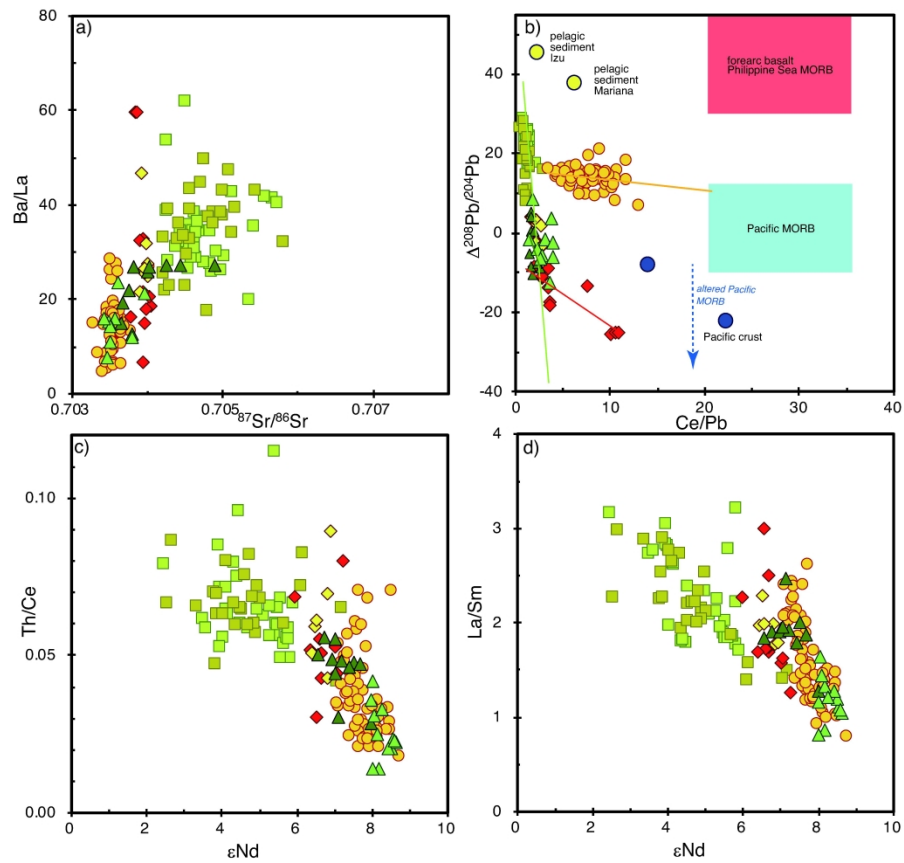


Fig. 7 Ishizuka et al.

Fig. 7. Isotope versus trace element ratio plots for the Bonin Islands volcanics. Data sources are the same as for Figure 6. Isotope versus trace element ratio plots for the Bonin Islands volcanics. Data sources are the same as for Figure 6. Least squares regression lines are shown in panel b. Symbols as in Fig. 4.

202x271mm (600 x 600 DPI)

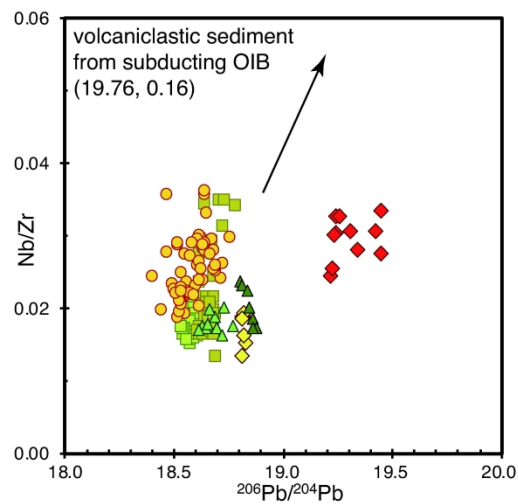


Fig. 8 Ishizuka et al.

Fig. 8. Nb/Zr vs. $^{206}\text{Pb}/^{204}\text{Pb}$ plot. A vector towards volcaniclastic sediment derived from HIMU oceanic islands is shown (Plank & Langmuir, 1998). Symbols as in Fig. 4.

168x235mm (600 x 600 DPI)

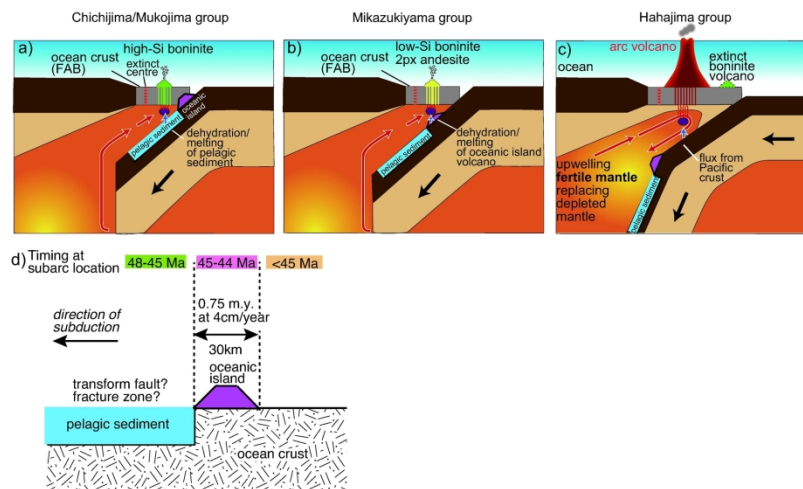


Fig. 9 Ishizuka et al.

Fig. 9. Schematic diagram showing the progressive variation in the nature of the slab flux following subduction initiation. a) Chichijima/Mukojima group, 48-45 Ma: shallow melting (~ 35 km) with flux from pelagic sediment and Pacific Ocean igneous crust added to a harzburgitic mantle; b) Mikazuki group, 45-44 Ma: melting at ~ 35 km, slightly further from the trench, flux from HIMU volcanoclastic sediment added to a less depleted mantle source; c) Hahajima group, <45 Ma: deeper melting (~ 60 km) further from the trench with flux from Pacific Ocean crust added to an upwelling, more fertile mantle source. d) Schematic diagram showing the estimated scale and duration of flux components on the subducting slab.

187x258mm (300 x 300 DPI)

Table 1 Results of $^{40}\text{Ar}/^{39}\text{Ar}$ dating of volcanic rocks from the Bonin islands.

Analysis No.	Sample No.	Name of island	steps	Total gas age ($\pm 1\sigma$)	Plateau age ($\pm 1\sigma$)				
				integrated age (Ma)	weighted average (Ma)	inv. isochron age (Ma)	$^{40}\text{Ar}/^{36}\text{Ar}$ intercept	MSWD	fraction of ^{39}Ar (%)
<i>Hahajima Island Group</i>									
09260	07112104-4	Hahajima	30	48.2 \pm 0.3	45.28\pm0.17	43.9 \pm 1.6	314 \pm 20	1.32	63.6
09261	05121801A	Hahajima	31	45.2 \pm 0.5	40.2\pm0.5	39.7 \pm 4.5	296 \pm 6	0.90	58.1
11316	10093001-1	Hahajima	15	44.16 \pm 0.25	42.66\pm0.18	41.4 \pm 0.5	592 \pm 85	1.16	81.7
09235	05122110	Meijima	15	42.0 \pm 0.4	38.4\pm0.4	35.2 \pm 2.1	340 \pm 28	0.73	38.7
08376	07032943-1	Imoutojima	14	40.2 \pm 0.9	39.8\pm0.7	38.7 \pm 1.2	334 \pm 26	1.18	78.8
11309	10092707-1	Mukoujima	19	41.2 \pm 0.3	44.6\pm0.4	42.8 \pm 1.3	348 \pm 37	0.57	31.6
<i>low-Si boninite from Chichijima Island Group</i>									
18172	06062604C	Otoutojima	19	44.57 \pm 0.19	45.16\pm0.15	45.3 \pm 0.3	292 \pm 6	1.24	89.3

inv. isochron age: inverse isochron age.

MSWD: mean square of weighted deviates $((\text{SUMS}/(n-2))^{0.5})$ in York (1969).

Integrated ages were calculated using sum of the total gas released.

$\lambda_b = 4.962 \times 10^{-10} \text{y}^{-1}$, $\lambda_e = 0.581 \times 10^{-10} \text{y}^{-1}$, $^{40}\text{K}/\text{K} = 0.01167\%$ (Steiger & Jager 1977).

Atmospheric $^{40}\text{Ar}/^{36}\text{Ar}$: 295.5